Development of ZBLAN Fiber-Based Components

Hsin-yu Lu

Department of Electrical and Computer Engineering

McGill University

Montreal, Quebec, Canada

December, 2011

A thesis submitted to McGill University in partial fulfillment of requirements

for the degree of Master of Engineering

Abstract

With a superior transmittance in the mid-infrared, fluoride fibers such as ZBLAN fibers can be used to develop fiber-based components for that spectrum. In this thesis, we investigate the fusion splicing of ZBLAN fibers as well as the fabrication of long-period gratings and Mach-Zehnder interferometer structures. Average losses in the range of 0.23-0.31 dB are achieved for the fusion splicing among multi-mode and single-mode ZBLAN fibers. In the C- and O-bands, notches of depths ranging from 6-17 dB are obtained with mechanically induced long-periog gratings. All-fiber Mach-Zehnder interferometers are also demonstrated by cascading the long-period gratings. An equation used to calculate the relation between the fringe spacing and the separation length shows that the smallest and the largest difference compared to the measurements are 1.81% and 7.37%, respectively.

Sommaire

Avec une transmission supérieure dans l’infrarouge moyen, des fibres de fluorure telles que des fibres de ZBLAN peuvent être employées pour développer les composants à fibres pour ce spectre. Dans cette mémoire, nous étudions les épissures ainsi que la fabrication des réseaux à long pas et des interféromètres Mach-Zehnder. Des pertes moyennes dans la gamme de 0.23-0.31 dB sont obtenues pour les épissures parmi des fibres multi-modales et unimodales. Dans les bandes C et O, la profondeur des bandes atténuées varie entre 6-17 dB avec des réseaux à long pas. Des interféromètres Mach-Zehnder sont également démontrés en cascadant les réseaux à long pas. Une équation pour calculer la relation entre l'espacement de frange et la longueur de séparation prouve que la plus petite et la plus grande différence comparée aux mesures sont 1.81% et 7.37%, respectivement.

Acknowledgments

The researches in this thesis would not be possible without Prof. Lawrence R. Chen’s guidance and support. I would like to thank my supervisor for teaching and motivating me during these years. Not only his knowledge, but his project management and pursuit of best results are also admirable. It is with great pleasure to work with him.

The ZBLAN optical fibers used in this thesis are provided by IRphotonics. I would like to thank Dr. Mohammed Saad, Ruben Burga, Antoine Kasprzak, Shane Dian, and everyone who have made working on this material possible. Patrick Orsini has given important information regarding the fiber.

A lot of equipment is from Optech in Montreal. I would like to thank Dr. Denis Lafrance, Dr. Robert Larose, and Mathieu Riendeau in that wonderful laboratory environment. Felix Fan has mentored me in my early days in the field of photonics, especially during the work of fusion splicing.

Former students from the photonics group also gave me critical advice and help towards the completion of mechanically induced gratings. I would like to thank Dr. Dominik Pudo for sharing his experiences. The good days of working with my other mentor, Rhys Adams, are memorable.

In the experiments involving doped ZBLAN fibers, I am thankful to work with Dr. Abdul Sarmani. In addition, I appreciate the insightful discussions with Wanjing Peng. I have learned a great deal from them and our talks are among my best times in the laboratory. My special thanks are for Chams Baker who glue-spliced our ZBLAN fibers.

The Photonics Systems Group in McGill University is a very friendly place to work. My thanks are to Dr. Pegah Seddighian, Zhaobing Tian, Yu Ping Zhang, Jia Li, Tianye Huang, Junjia Wang, and Lv Zhang who helped me with equipment and with whom I had inspiring discussions. Maria-Iulia Comanici's help in Ottawa is really appreciated.

I would like to thank the Canadian Institute for Photonic Innovations, the Natural Sciences and Engineering Research Council of Canada, and McGill University for their supports.

I would like to thank my grandmother, parents, brother, family, and friends for supporting me all these years. Certainly, my grandmother and parents are the most important people to thank in all kinds of my lists. Many thanks are for Jay Lu who always guided and participated in my non-academic activities. Yi-chen Li is the reason that keeps me going.

Table of Contents

List of Figures

List of Tables

List of Acronyms

IR	Infrared
QCL	Quantum Cascade Laser
LPG	Long-Period Grating
MZI	Mach-Zehnder Interferometer
HMF	Heavy Metal Fluoride
MM	Multi-Mode
NA	Numerical Aperture
SM	Single-Mode
CCD	Charge-Coupled Device
FBG	Fiber Bragg Grating
UV	Ultraviolet
ELED	Edge-emitting Light Emitting Diode
BBS	Broad-Band Source
BS	Beam Splitter
PCF	Photonic Crystal Fiber

SOA	Semiconductor Optical Amplifier
EDFA	Erbium-Doped Fiber Amplifier
OSA	Optical Spectrum Analyzer
UTS	Unified Thread Standard
ASE	Amplified Spontaneous Emission
SMF	Single-Mode Fiber

Chapter 1 - Introduction

From a general point of view, tools based on the use of light are everywhere in human civilizations in the known past, present, and will not be absent in the imaginable future. One of the fundamental uses is illumination. Waves and particles within human visible range show the world to eyes and then consciousness. The development of the light tools does not stop here and continues to make lives easier in many more types of domains.

Photonics gained increasing attention after the invention of the laser as a light source and optical fiber as transmission medium. Its applications are not restricted to visible spectrum and they extend to sensing, micromachining, medicine, telecommunications, and more [1]. Researchers of this field work on transmission, generation, modulation, detection, amplification, processing, and developing systems of light. This thesis research focuses on the aspects of the transmission, processing, and generation of light in fluoride glass.

1.1 Objectives and Motivation

The research objective is to develop fiber-based components using ZBLAN (fluoride glass) fiber. In short, ZBLAN fiber, as a medium, is a good candidate to build upon both active and passive components for the mid-infrared (mid-IR). To further clarify the purpose, a comparison of ZBLAN fibers to the currently deployed silica fibers and an overview of mid-IR applications are presented. The studied aspects are fusion spliced joints (light transmission), long-period grating (light processing), Mach-Zehnder interferometer (light processing), and linear cavity fiber laser (light generation).

Conventional optical fiber is made of silica (SiO_2) glass. Three important properties make this type of fiber popular in the field of photonics [2]. The first property is its viscosity can be well controlled at an accessible range of temperatures. Fabrication with this already widespread material becomes even easier. The second property is the optical transparency window which allows applications in various wavelength ranges. Around the 1.5 μm wavelength, its attenuation can be as low as 0.2 dB/km. The third property is the strong intrinsic strength. It can be comparable to a steel wire of the same diameter if the fiber is well polished and protected. These three properties make silica fiber a favorite in the field of photonics.

The question is why research on other materials is needed if silica technology is so successful. Other materials often suffer from more difficult fabrication processes and weaker strengths. The current fluoride fiber is one of them. Its best known limiting factors are cost and fragility. Despite several disadvantages compared to a mature fiber, it stands out in other aspects.

In terms of the optical transparency window, fluoride fiber is superior to silica fiber in theory. Fluoride glass can have transmission range from ~0.3 μm to

~7 μm wavelength depending on compositions [3]. Fig. 1.1 illustrates that ZBLAN has lower loss over a wider range of wavelengths compared to silica. Around 1.5 μm, attenuation in silica fiber is below ~0.2 dB/km. It suffers from increasing loss beyond 2 μm. On the other hand, attenuation in ZBLAN is not only similar to that of silica from 0.3 μm to 1.5 μm, but is lower at longer wavelengths. Its lowest loss range is between 2.5 μm and 3 μm. 3 μm (2 μm sometimes) to 8 μm is usually considered the mid-IR range. With the better loss performance in a range that silica fails to deliver, ZBLAN is preferred as the material to use in the mid-IR.

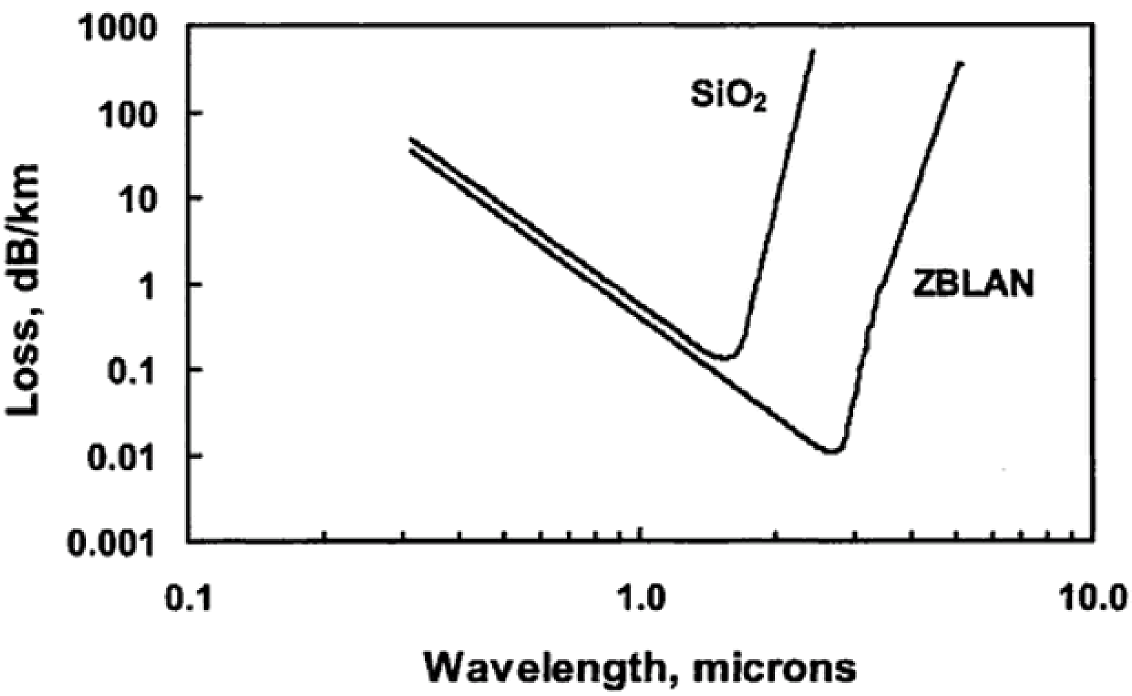

Figure 3.1: Intrinsic loss comparison between silica and ZBLAN glasses [4]

Table 1.1 compares the parameters of silica and ZBLAN glass. One of the notable properties is the transition temperature T_g. It is an important factor that differentiates these two materials in fusion splicing settings. The lower T_g is, the lower temperature it takes to fuse. The Young's modulus indicates the lower stiffness in ZBLAN. The refractive indices are also noteworthy because their similarity allows lower coupling losses between silica and ZBLAN.

Property	ZBLAN	Silica glass
T_g, °C	259	1175
Specific heat, cal/g °C	0.151	0.179
Thermal conductivity, W/m °C	0.628	1.38
Expansion coefficient	17.2×10^{-6}	0.55×10^{-6}
Density, g/cm^3	4.33	2.20
Knoop hardness, kg/mm^2	225	600
Toughness (K_{IC}), MPa m$^{1/2}$	~0.32	0.72
Young's modulus, GPa	52.7	72.2
Poisson's ratio	0.31	0.17
Refractive index (0.59 μn)	1.499	1.458
Abbe number	76	68
ZMD wavelength, μm	1.6	1.3
dn/dT, °C^{-1}	-14.75×10^{-6}	$+11.9 \times 10^{-6}$
Minimum intrinsic loss, dB/km	0.01 (2.55 μm)	0.14 (1.55 μm)
Lowest measured loss, dB/km	0.45 (2.3 μm)	0.16 (1.55 μm)

Table 2.1: Parameter comparison between silica and ZBLAN glasses [4]

In order to further justify the research motivation, an overview of potential applications by ZBLAN fiber components is briefly presented. In general, fluoride fibers are suitable for chemical sensing, thermal imaging, fiber lasers, and other mid-IR applications. Three fields with the demands in the mid-IR are presented: Free-space communication, sensing, and medicine.

A mid-IR transmitter is typically favourable in free-space communication because its loss is reduced in atmosphere compared to that of a source operating at 1.5 μm [25]. For example, several groups have studied the performance of mid-IR (e.g., 3.8 μm or beyond 8.1 μm) and near-IR (0.85 μm) sources for use in free-space communications and confirm the superiority using the former [26-28]. Typically, quantum cascade lasers (QCLs) are used as the mid-IR transmitters. Although the optimized wavelengths (for free space communications) of 9-13 μm are beyond the wavelength range of ZBLAN fiber, ZBLAN fiber lasers are a potential alternative at 3.8 μm.

In terms of sensing, it is reported that mid-IR (8-8.5 μm) emission can be used to analyze earthquakes [29]. Furthermore, there are discussions of mid-IR sensors for gas analysis [30] and environmental monitoring [34]. A research group has demonstrated a room-temperature mid-IR (4.6 μm) laser sensor for trace gas detection [31]. There are also other gas sensors at 5.2 μm [32] and around 3.3 μm [33, 35]. M. Saito *et al.* prepared a table of reported fiber-based chemical sensors in 1997 [36]. Commonly speaking, there is research on mid-IR spectroscopy in astronomy and food science as well.

Mid-IR is also used for medicine. For example, it can be applied to imaging of biological tissues [37]. Mid-IR laser at 5.2 μm can be used to analyze human breath [38]. There are discussions of mid-IR laser applications in medicine [39, 43] and it can be used for ablation [44-45].

With the available equipment, all experiments of this thesis are conducted within the near-IR. Fusion splicing allows transmission between ZBLAN fibers or between two different fibers. After being able to fusion splice them, it also becomes possible to shape ZBLAN in order to make more components such as couplers. Long-period gratings (LPGs) function as wavelength-selective filters. They can be handy tools in signal processing when certain wavelengths need to be filtered. Furthermore, a Mach-Zehnder interferometer (MZI) can function as a multi-spectral filter. It is also useful in signal processing within ZBLAN fibers.

1.2 Organization

In chapter 2, a description of ZBLAN fiber is briefly presented. A comparison among the loss performances of the ZBLAN fibers fabricated by different groups is given. Next, a typical procedure of fusion splicing is introduced. The splicing losses are reviewed among the fusion splicing of ZBLAN fibers from different groups. In addition, the operation principles of LPGs, MZIs, and fiber lasers are introduced and followed by the all-fiber solutions from different groups.

In chapter 3, basic handling of ZBLAN fibers is introduced. Preparations before the fusion splicing such as stripping and cleaving are also presented. The average losses, minimum losses, and fiber strengths of the fusion splicing among ZBLAN fibers are discussed.

In the chapter 4, the fabrication and the setup of mechanically-induced LPGs are described. Furthermore, the resulting spectral responses are shown and the measured results are compared to simulations of LPGs.

In the chapter 5, the setup of ZBLAN MZIs based on cascaded LPGs is explained. The resulting interference patterns are analyzed.

In the chapter 6, a summary of the thesis is provided. Future work is also discussed.

1.3 Contribution

Some of the results presented in this thesis can be found in the following publications:

- H.-Y. Lu, R. Adams, M. Saad, P. Orsini, R. Burga, and L. R. Chen, "Mechanically induced long period gratings in ZBLAN fibers," Information Photonics, 18 - 20 May 2011, Ottawa, Ontario.
- H.-Y. Lu, R. Adams, M. Saad, P. Orsini, R. Burga, and L. R. Chen, "Mechanically induced and cascaded long period gratings in ZBLAN fibers," IEEE Photonics Conference, 9-13 October 2011, Arlington, VA.

Chapter 2 - Background and Review

2.1 ZBLAN Fiber

The word “ZBLAN” comes from the initials of ZrF_4-BaF_2-LaF_3-AlF_3-NaF. The elements are zirconium (Zr), barium (Ba), lanthanum (La), aluminum (Al), and sodium (Na) combined with fluorine (F). It is part of the heavy metal fluoride (HMF) glass family. The HMF glasses were researched by Poulain and Lucas around 1974 [5]. At University of Rennes in 1975, they accidentally discovered HMF based on zirconium fluoride, also known as fluorozirconate fluoride glasses. Compared to other mid-IR fibers such as chalcogenide fiber, ZBLAN has a refractive index that is closer to that of silica. The high refractive index of chalcogenide can cause higher loss at a glass-air interface. Among the HMF family, ZBLAN is one of the most popular materials nowadays because of its better stability and easier fabrication.

Contrary to the theory, the measured loss of ZBLAN fibers is not better than that of silica fibers in practice, as shown in Table 1.1. In principle, the intrinsic loss of ZBLAN is lower than that of silica. However, extrinsic loss still dominates the total loss. To achieve better transmission performance, research groups have worked to improve the fabrication process. Carter *et al.* at British Telecom Research Laboratories demonstrated one of the lowest ZBLAN fiber losses. The fiber is multi-mode with a 70 μm core diameter and 150 μm cladding diameter. Fig. 2.1 shows the transmission spectrum from 0.5 μm to 3.5 μm. The lowest loss is 0.65 ± 0.25 dB/km at 2.59 μm. Out of this total loss, they report that extrinsic absorption contributes 0.33 dB/km and a total scattering loss contributes 0.30 dB/km. The ions shown in Fig. 2.1 are the impurities that cause the extrinsic absorption losses. The dotted line shows a mostly wavelength-independent scattering loss. To summarize, a very low-loss ZBLAN fiber is demonstrated in a laboratory environment.

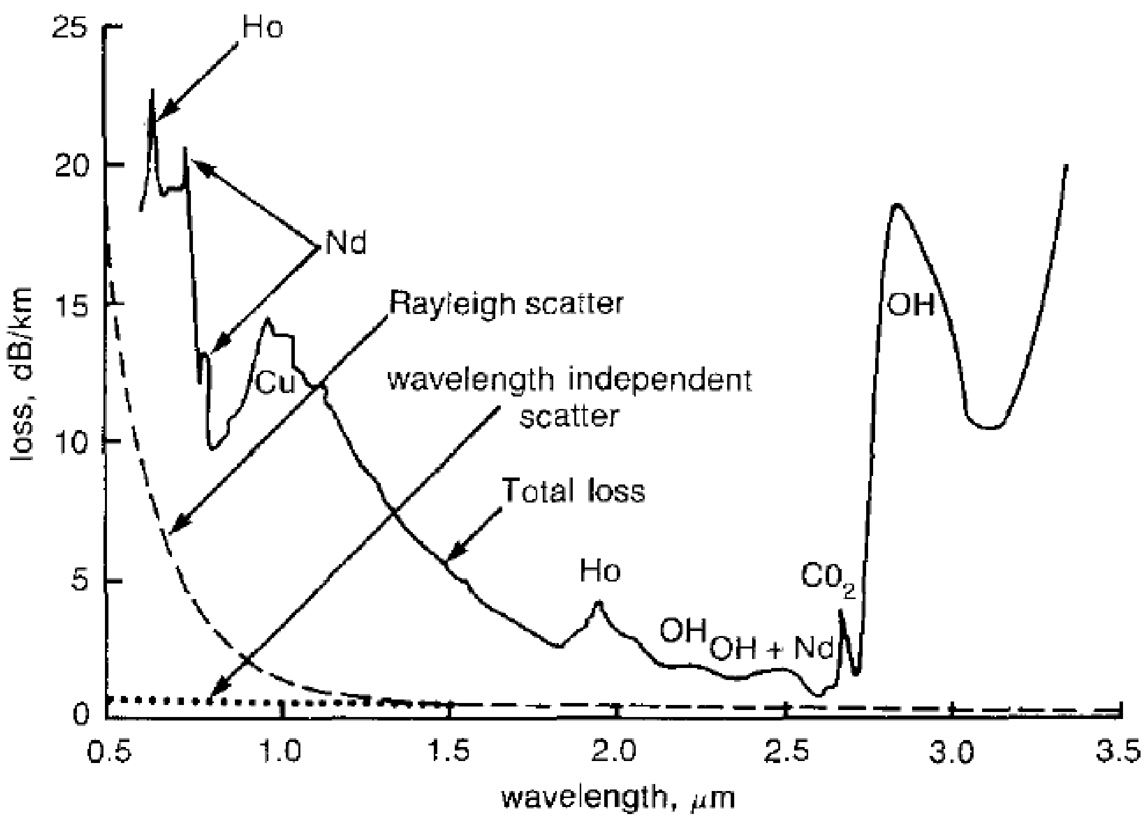

Figure 2.1: Measured lowest-loss ZBLAN fiber [6]

In terms of commercial production, 0.05 dB/m or 50 dB/km at ~2.5 μm is considered low loss. The loss of commercial ZBLAN fiber is about 100 times greater than of fiber fabricated in the laboratory. Since short-distance applications are the goals, such loss over 2-3 meters is acceptable. Fig. 2.2 records two examples of commercial ZBLAN fibers. These fibers have a minimum loss around 0.05 dB/m with losses under 1 dB/m over 0.5-4.5 μm, are multi-mode (MM) with an NA of 0.12-0.2, and are acrylate coated. Again, this range indicates the superior transmission of ZBLAN fiber over silica fiber especially from 3-5 μm.

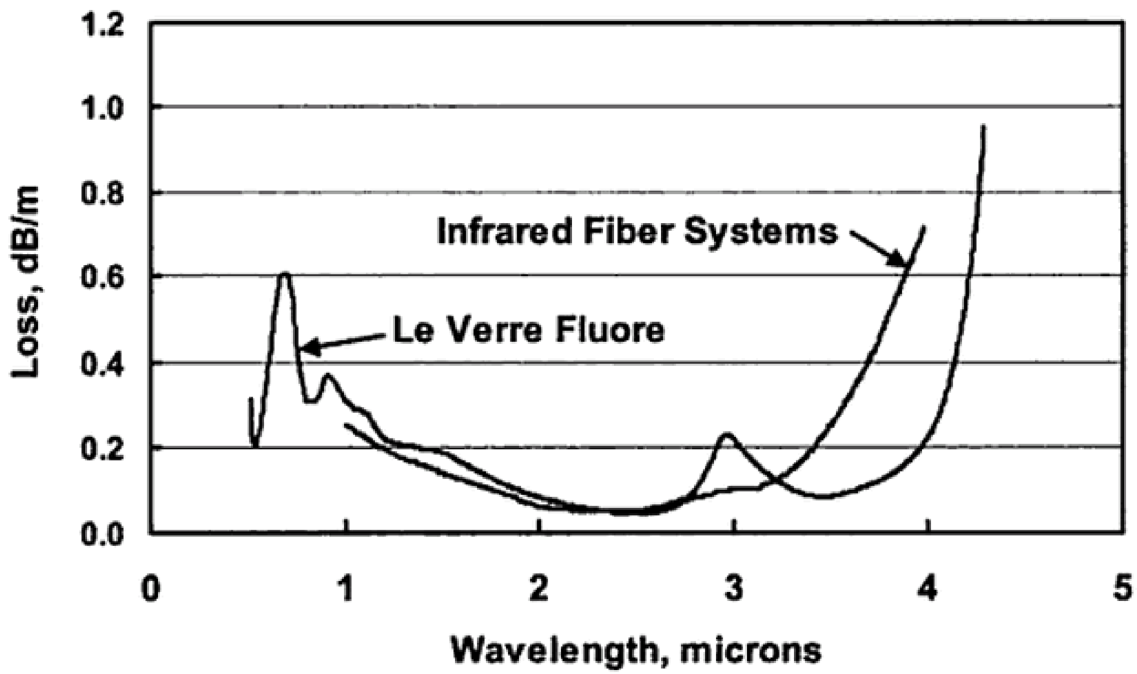

Figure 2.2: Spectral loss of commercial ZBLAN fibers [4]

All the ZBLAN fibers used in this thesis are manufactured and provided by IRphotonics. Fig. 2.3 shows the spectral attenuation of undoped MM ZBLAN fiber from IRphotonics. It has an attenuation below 1 dB/m from 0.4 μm to around 3.15 μm, a core diameter of 85 ± 7 μm, and a cladding diameter of 125 ± 2 μm. Its acrylate buffer diameter is 260 ± 15 μm. The breaking bend radius is 4 mm and the numerical aperture (NA) is 0.2. The operating temperature is from -20°C to 90°C. Fig. 2.4 shows the refractive index profile of a MM ZBLAN fiber with a core diameter "a" of 74 μm and a NA of 0.198. The core index is close to 1.494 and the cladding index is around 1.481.One of the main failures that a spliced joint can have is mechanical fracture [11]. Proof testing is done to ensure the mechanical robustness and long-term reliability of a splice. It typically has three stages: (1) increasing the tension of the splice joint, (2) holding the joint at the tension for a time interval, and (3) decreasing the tension back to zero. The resulting value is the measured maximum tension under which a joint can last. The proof test result is above 50 kpsi.

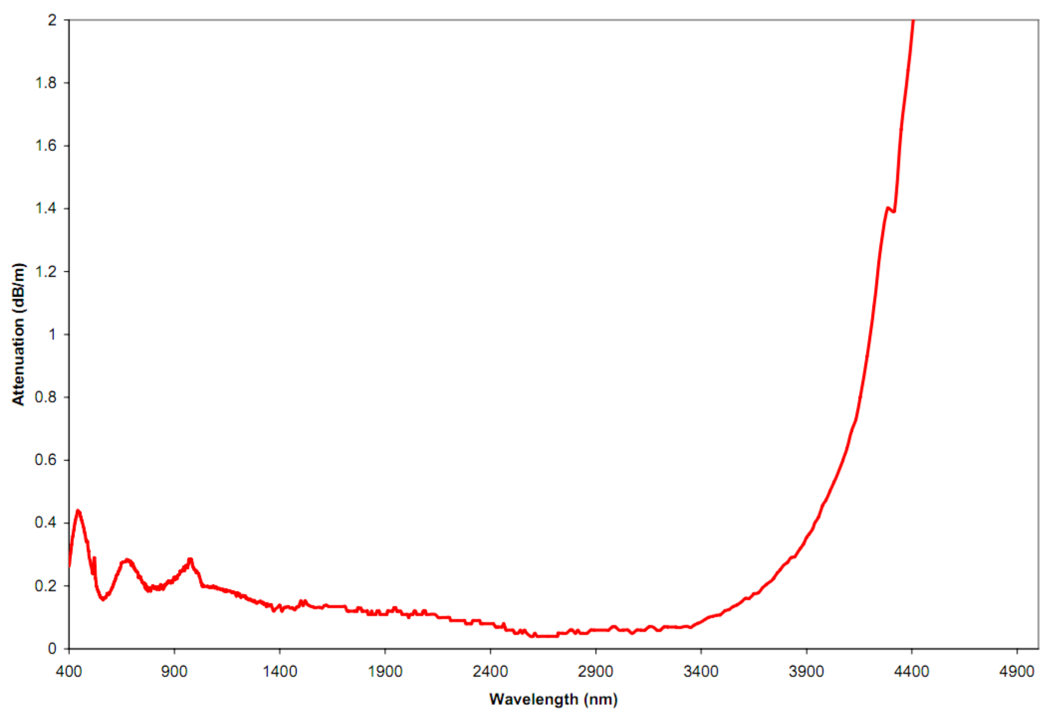

Figure 2.3: Spectral attenuation of undoped multi-mode ZBLAN fiber made by IRphotonics [8]

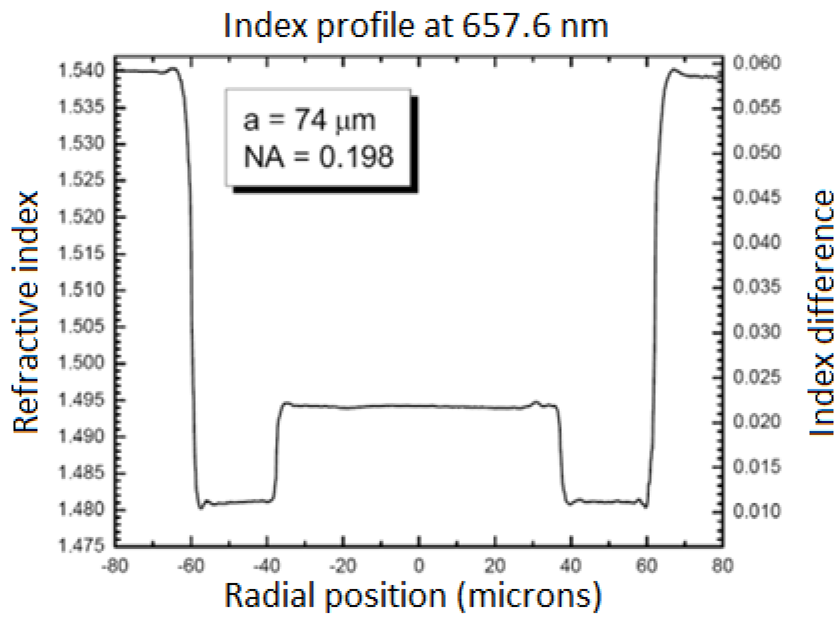

Figure 2.4: MM ZBLAN fiber refractive index profile by IRphotonics [10]

The undoped single-mode (SM) ZBLAN fiber from IRphotonics has a core diameter of 9 μm and cladding diameter of 125 μm [9]. The coating is acrylate. The breaking bend radius is 2 mm and the NA is 0.17. For this NA, the SM operating wavelength range is above 2 μm. Since the experiments of this thesis use wavelengths below 2 μm, the fiber operates in the MM regime (Appendix C). The fiber has a transmission range of 0.3-4.5 μm, an operating temperature from -20°C to 90°C, a proof test result above 50 kpsi and an attenuation of 0.19 dB/m at 1.5 μm. Fig. 2.5 shows the refractive index profile of the SM ZBLAN fibers. The core has an index around 1.491 and the cladding index is close to 1.476.

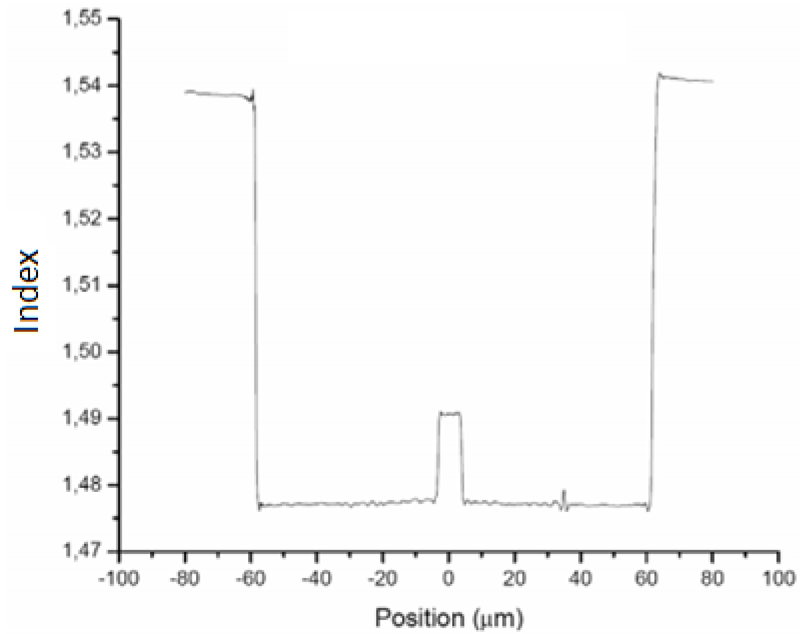

Figure 2.5: SM ZBLAN fiber refractive index profile by IRphotonics [10]

2.2 Fusion Splicing

The goal of optical fiber fusion splicing is to make a permanent, low-loss, high-strength, welded fiber joint. In other words, separated fibers are connected to each other in a way as if they were never separated. Splicing involves several steps, as shown in Fig. 2.6. The first step is to remove the protective coating of the fiber by stripping. The stripped part should be cleaned with alcohol to avoid any dust or dirt. The second step is to cleave the stripped fiber to achieve an end surface that is as flat as possible. The third step is to align the two separated fiber ends by motorized stages in a fusion splicer (See Fig. 2.7). Motorized alignment ensures the best position prior to heating. A charge-coupled device (CCD) camera is used to provide visual inspection to users and also to the microprocessor. After the alignment is finished, a heat zone around the tips is generated. Generally, there are two types of heat sources: arc and filament. During the heating, the motors can push, pull, or perform more actions to achieve the desired effects. The fiber tips become soft and link to each other. In the fourth step, a joint is formed after heating. The fifth and sixth steps are to measure the loss and strength performances, respectively. The splice is protected to ensure longer lifetime in the seventh step. Finally, a fusion splice is completed.

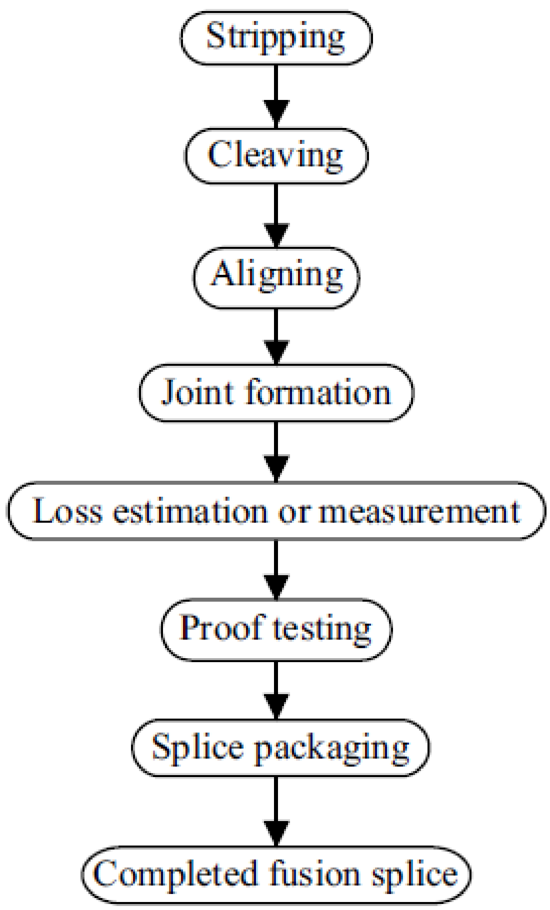

Figure 2.6: Steps in optical fiber fusion splicing [11]

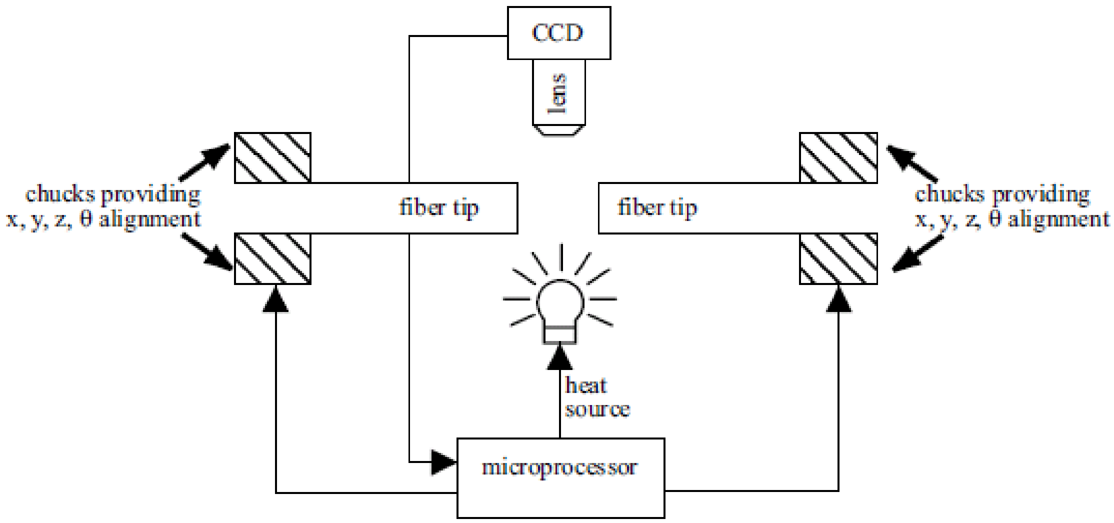

Figure 2.7: Schematic of fusion splicer [11]

Fig. 2.8 shows an example of a completed fusion splice. These images are the visual inspection provided by the CCD camera to users. Fig. 2.8 (a) shows the third step where alignment occurs, Fig. 2.8 (b) shows the push during heating, and Fig. 2.8 (c) shows the final splice.

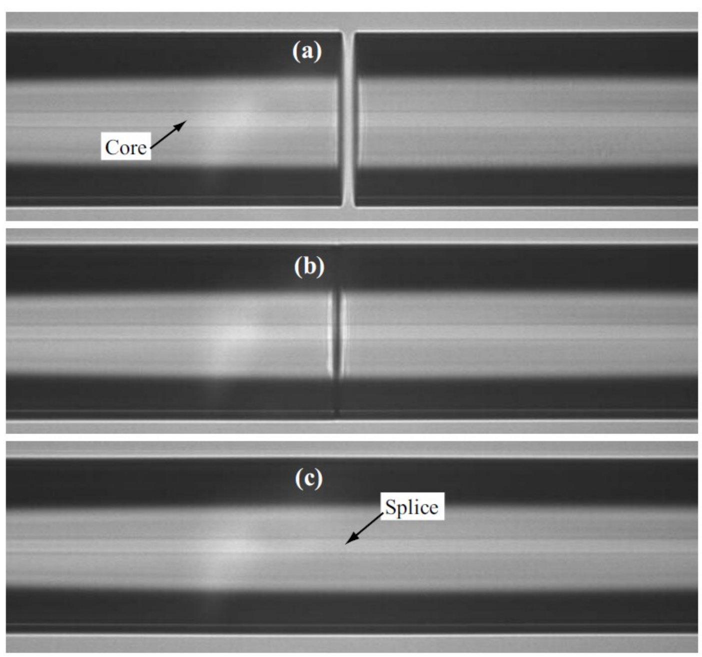

Figure 2.8: Example of fusion splice (a) aligned (2) hot pushed (3) completed [11]

Several research groups have demonstrated fusion splicing with ZBLAN fibers. Harbison *et al.* uses a spool of MM ZBLAN fibers with 40 μm core diameter, 125 μm cladding diameter, and 0.14 NA. Their splicer is an arc fusion splicer from Power Technologies Inc. (Model: PTS-330) [12]. They set the arc ramped to a current level of ~7 mA for 0.1-1.0 second. Fig. 2.9 shows their splice loss histogram. Out of 35 splices, an average loss of 0.25 dB is obtained, where the minimum loss is 0.05 dB.

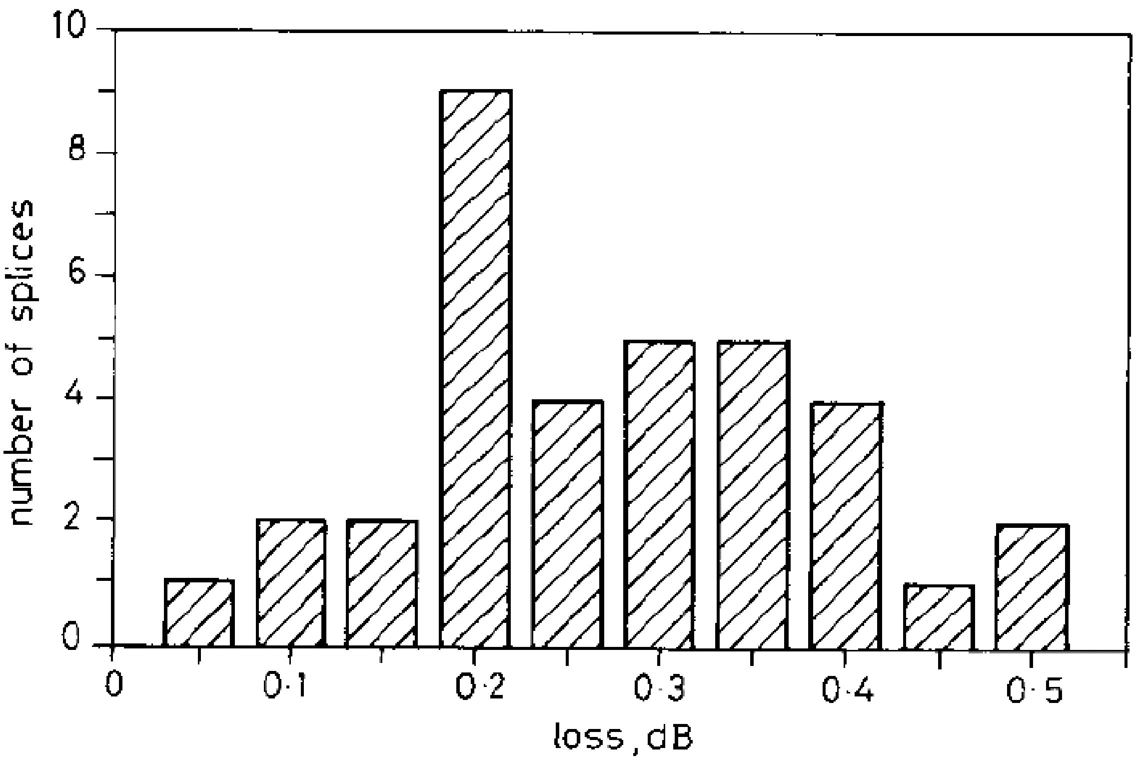

Figure 2.9: Fusion splices loss of ZBLAN fibers by Harbison *et al.* [12]

By using another type of heat source, namely a filament, Srinivasan *et al.* have demonstrated ZBLAN fusion splicing as well [13]. Their ZBLAN fiber has a

15 μm core diameter. Out of 5 splices, an average loss of 0.3 dB and a lowest loss of 0.08 dB are achieved.

Pei *et al*. have demonstrated fusion splicing between ZBLAN and silica fibers using an arc fusion splicer [14]. The splicer in use is an FSM-20PM Arc Fusion Splicer. Their best result is a splice loss of 1.58 dB.

2.3 Photoinduced Fibre Grating Structures in ZBLAN Fibers

Several methods can be used to write fiber gratings in ZBLAN fibers, including those based on ultraviolet (UV) exposure and laser inscription. Poignat *et al*. reported fiber Bragg gratings (FBGs) at 1.55 μm with UV exposure at 246 nm [46]. A transverse holographic method is used. The fiber used is Cerium-doped and composed of ZBLALi. It has an NA of 0.22 and a core diameter varied between 2.5 and 4 μm. They achieved a maximum index modulation of $4 \cdot 10^{-4}$ by increasing the Cerium concentration. A peak reflectivity of 95% with a grating length of 5.1 mm is reported. Taunay *et al*. showed UV-induced FBG in Cerium-doped ZBLAN [47]. A holographic method is used. Their fiber has a cerium concentration of 10000 ppm and a core diameter of 5 μm. A permanent change in the refractive index of $2 \cdot 10^{-5}$ at 1560 nm is achieved. A peak reflectivity of 10% with a length of 10.3 mm is reported.

More recently, Grobnic *et al*. presented FBGs in undoped ZBLAN fibers by femtosecond near-IR laser inscription at 800 nm and a phase mask [48]. Their fibers are SM with a core diameter of 4 μm and MM with a core diameter of 50 μm. A ~46% reflecting grating and a modulation of at least $2 \cdot 10^{-4}$ are achieved in the SM fiber. A maximum reflectivity of ~2% for the MM fiber is measured. Bernier *et al.* also developed FBG in ZBLAN fibers by femtosecond laser at 800 nm and a phase mask [49]. Their fibers are SM thulium-doped and SM undoped. A maximum index modulation of the order of 10^{-3} is achieved for both types of fibers. A peak reflectivity that is close to 100% at a grating length of ~4.5 mm is reported.

2.4 Long-Period Grating

Physically, an LPG is a periodic perturbation in the refractive index along the longitudinal axis of the fiber. It has the same function as a band-rejection filter. It causes a set of spiky losses at different wavelengths in the transmission spectrum [15] and is usually on the orders of hundreds of μm. The name “long-period” comes from the fact that its period is longer than that of typical FBG. Instead of having back reflections as in an FBG, in an LPG, the core mode is coupled to forward-propagating cladding modes. That is, modes of certain wavelengths in the core are coupled to the cladding, as illustrated in Fig. 2.10.

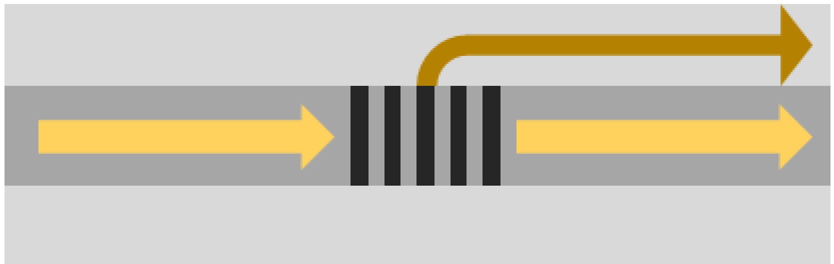

Figure 2.10: Co-propagating modes in LPG

Eq. 2.1 gives the wavelengths λ_m where the stop-bands can be found:

$$\lambda_m = \Lambda(n_{core} - n_{cl}^m) \qquad (2.1)$$

where Λ is the grating period, n_{core} is the effective index of the fundamental mode, and n_{cl}^m is the effective index of the m-th cladding mode [16]. A typical spectral response of an LPG formed by UV exposure is shown in Fig. 2.11. A set of stop-bands appear corresponding to coupling from the core mode to several cladding modes.

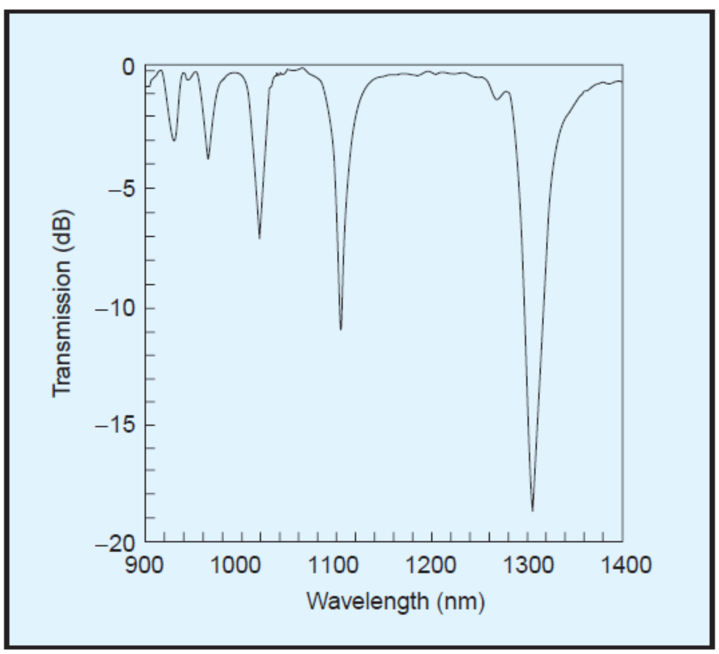

Figure 2.11: Typical spectrum of long-period grating [15]

Other fabrication methods have emerged over the years. Savin *et al.* fabricated LPGs on conventional silica fibers using the periodic peaks from a grooved plate [16]. Since the period in a LPG is on the order of hundreds of micrometers, inducing it mechanically is feasible. By the photoelastic effect, pressing the fiber between a periodically grooved plate and a flat plate induces a periodic perturbation.

In their experiment, the fiber is Corning SMF-28 CPC single-mode fiber. It has a core diameter of 8.3 μm, cladding diameter of 125 μm, and NA of 0.11. As shown in Fig. 2.12, a section of the silica fiber rests in a flat plate while a grooved plate with a period of 712 μm is placed onto it. The protective fiber jacket is kept. Pressure on the grooved plate can be adjusted. Fig. 2.13 shows their experimental result. As the pressure increases, the notch depths vary. Their typical out-of-band loss is below 0.5 dB.

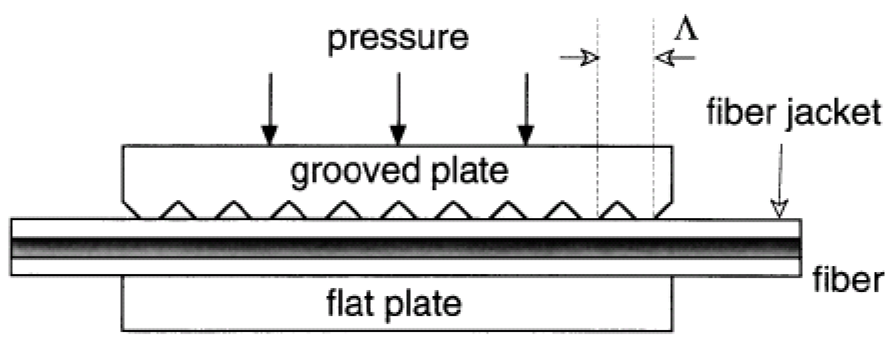

Figure 2.12: Experimental setup of silica fiber LPG by Savin *et al*. [16]

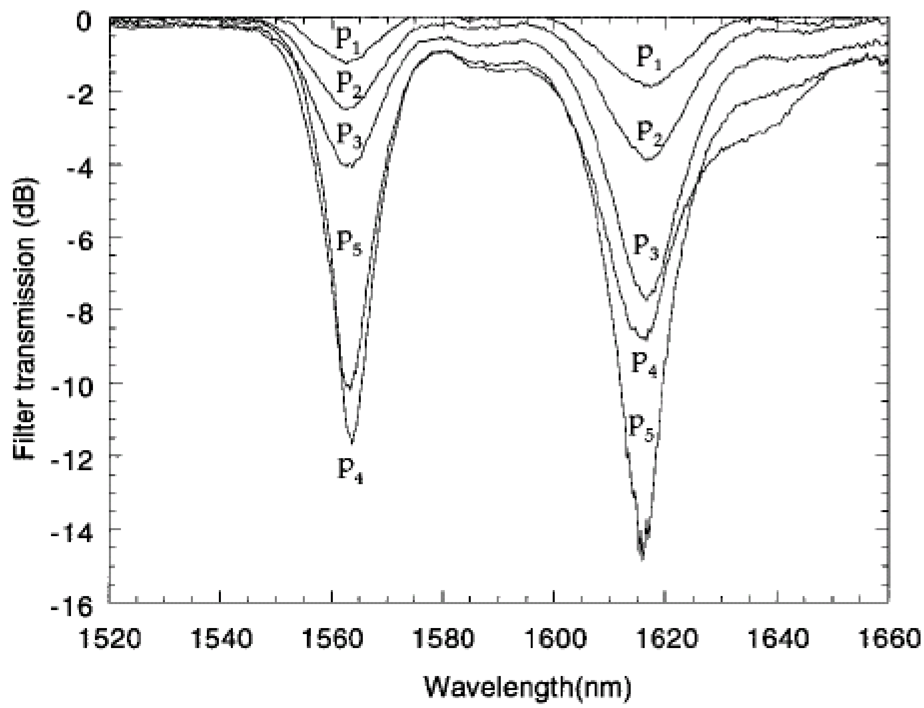

Figure 2.13: Response of the long-period grating with a 712-µm period and increasing pressures P_1-P_5 by Savin *et al*. [16]

This fabrication method has advantages over photoinduced LPGs. The latter is known for having low loss and flexibility in filter shape. The mechanically induced LPG not only inherits comparable low loss, but is also less expensive and simpler to make. Another advantage is that the grating is reversible as the index modulation disappears if the pressure is removed. After having successful results on the most matured silica fiber technology, researchers continue to make LPGs on other types of fibers.

Pudo *et al*. mechanically induced LPGs on chalcogenide fibers [17]. The fiber is single-mode, has 6 µm core diameter, core/cladding refractive index of 2.8, and 0.18 NA at 1550 nm wavelength. Instead of using a grooved plate, they used a threaded steel rod. The rod is 50 mm long, has a period of 0.7 mm, and a groove depth of 0.4 mm. The fiber jacket is also kept. A clamp is used to press the fiber between the rod and the plate, as shown in Fig. 2.14. An unpolarized edge-emitting light emitting diode (ELED) is used as a broad-band source (BBS). Two silica SMF are connected between the chalcogenide fiber and the equipment. Two 3-axis stages are used to adjust the fiber positions. The SMFs are butt-coupled with index-matching oil to the high NA chalcogenide fibers.

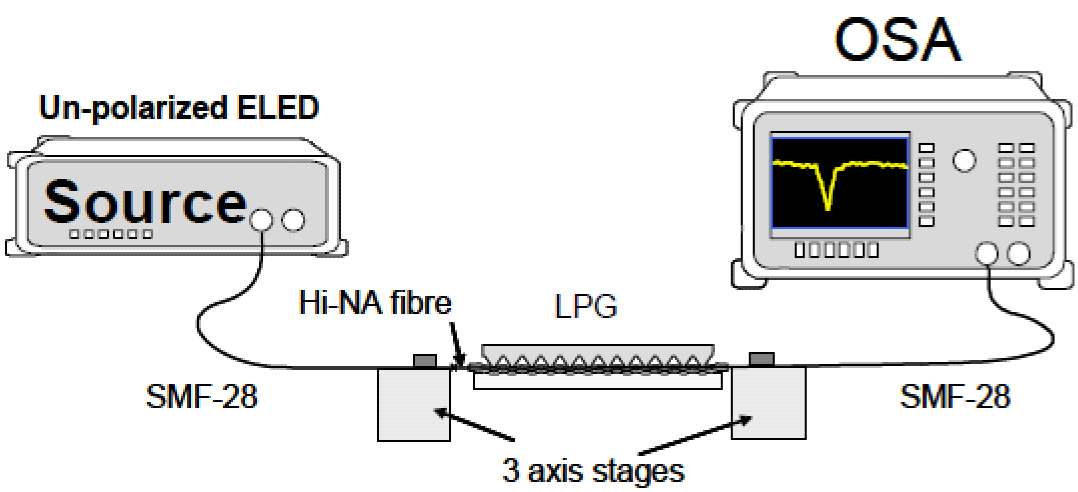

Figure 2.14: Experimental setup of chalcogenide fiber LPG by Pudo *et al*. [17]

Fig. 2.15 depicts the result of LPG fabricated in chalcogenide fibers with increasing clamp pressure. A peak attenuation of 22 dB and an out-of-band loss of less than 0.5 dB are obtained. Because chalcogenide fiber is similar to ZBLAN fiber in terms of fiber strength, the fact that a chalcogenide fiber LPG can be mechanically induced is encouraging for mechanically inducing LPGs in ZBLAN fiber.

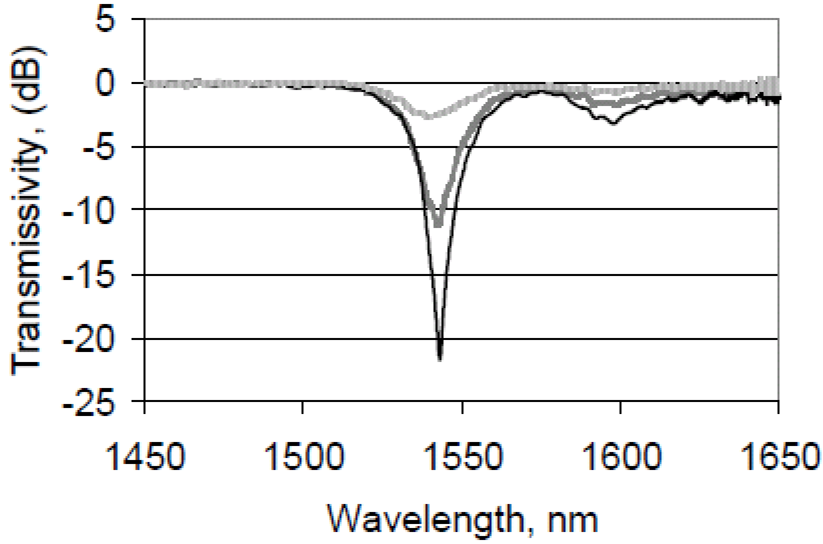

Figure 2.15: Result of chalcogenide fiber LPG with increasing pressure by Pudo *et al*. [17]

2.5 Mach Zehnder Interferometer

In a free-space setting, a MZI consists of two beam splitters (BS) and two mirrors (M) as shown in Fig. 2.16 [18-19]. The BS are used to split and recombine the beams. By adjusting the mirror position, the optical path lengths can be different for each arm. This difference determines the interference that occurs upon recombination. A similar concept can be applied to cascaded LPGs. The LPGs serve as BS where two different optical paths are created (for light propagating in the core and cladding) and the separation distance between the LPGs is analogous to the mirror position.

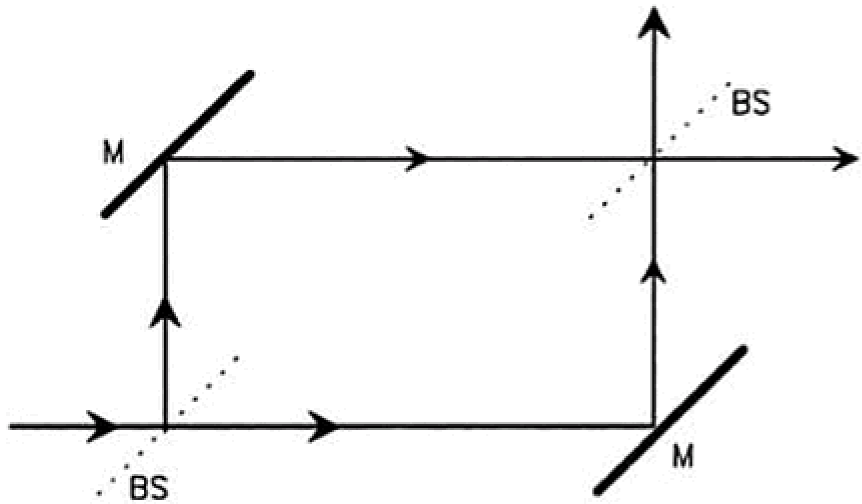

Figure 2.16: Operation principle of a Mach Zehnder interferometer [18]

As illustrated in Fig. 2.17, the basic idea of cascading two LPGs begins with the fact that the first LPG couples certain wavelengths from the core to the cladding. The core and cladding modes co-propagate for a length of separation between the gratings. After propagating through the separation, the optical path or relative phase differences between the core and cladding modes interfere at the recombination point. The second LPG serves as the recombination point of coupling certain wavelengths back to the core. The notches (coupled wavelength ranges) in the two LPGs should overlap to have an interference effect.

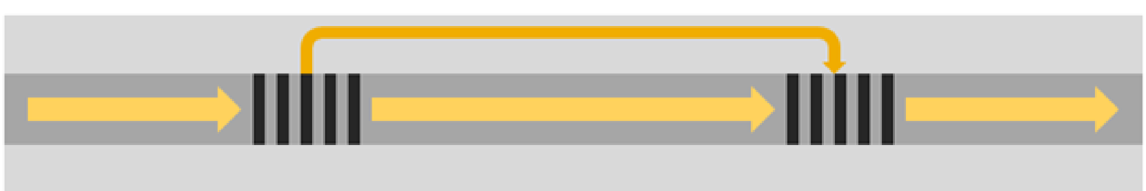

Figure 2.17: Operation Principle of Cascaded Long-Period Gratings

With photoinduced, identical, and cascaded LPGs, Gu demonstrated an MZI in conventional silica single-mode fiber (SMF) [20]. The LPGs are ~1 - 1.5 cm in length with a grating period of 450 μm. One trial has two 1 cm LPGs separated by 20 cm. The results are shown in Fig. 2.18. The wavelength spacing and the linewidth of loss peaks can be reduced by increasing the separation length.

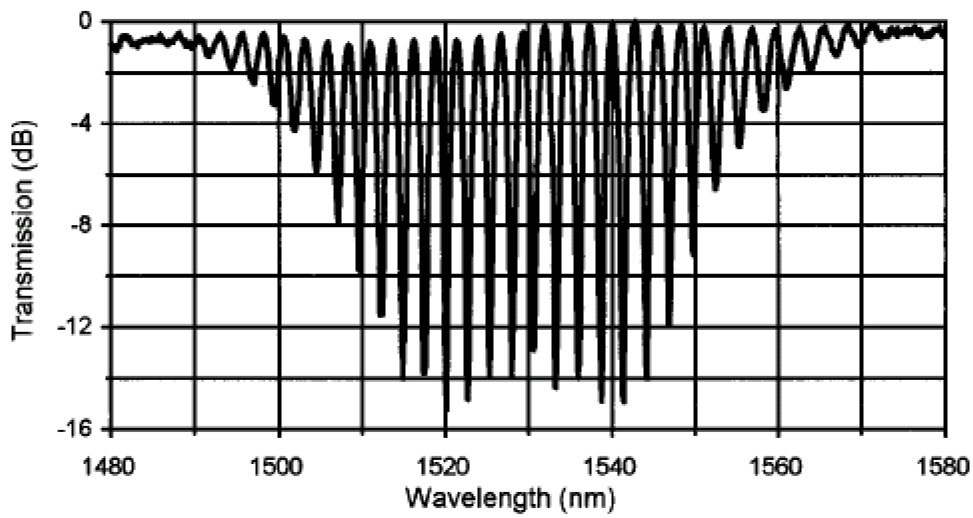

Figure 2.18: Experimental result of Mach-Zehnder interferometer based on cascaded long-period gratings by Gu [20]

Cascaded LPGs are also found in photonic crystal fibers (PCF). Lim *et al.* fabricated a MZI on PCF based on identical, cascaded, and mechanically induced LPGs [21]. Their PCF has a silica core diameter of 15 μm and airhole spacing of around 10 μm. The airhole diameter is around 5 μm. Fig. 2.19 shows their result without fiber coating. The grating period is 600 μm and grating length is 20 mm. With a separation length of around 5.5 cm, the fringe spacing is measured to be about 13.6 nm. Lim *et al*. also report that this spacing decreases with increasing grating separation.

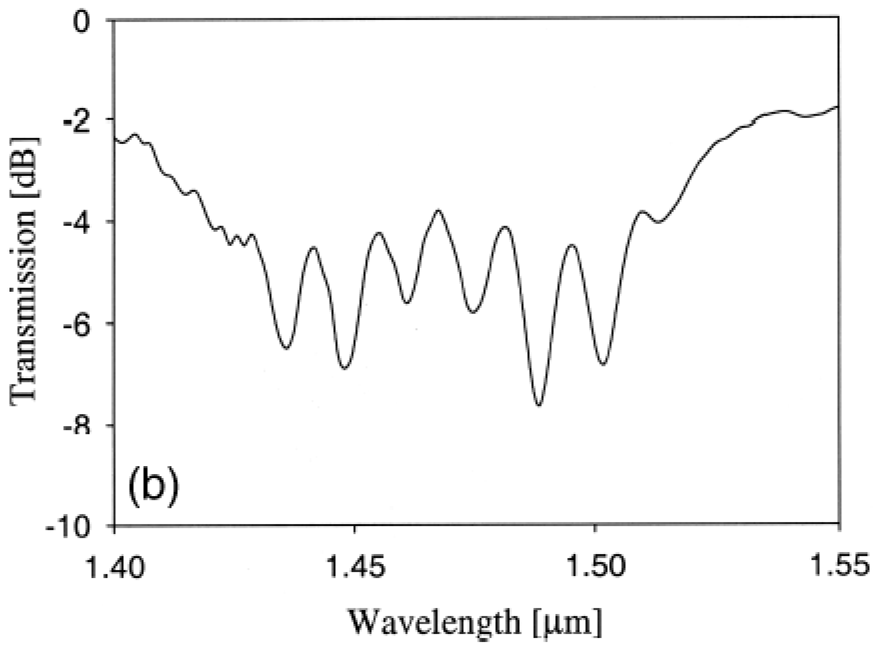

Figure 2.19: Cascaded long-period gratings on photonic crystal fiber by Lim *et al*. [21]

Instead of using cascaded LPGs to achieve MZI-like results, Choi *et al*. demonstrate an all-fiber MZI with one LPG followed by one point collapsing of air holes, where the two paths recombine [22]. The first split point is wavelength-selective as it is an LPG. The recombination point is not wavelength-selective, but the recoupled beam still interferes with the beam in the core. Fig. 2.20 presents the result of the single LPG in dashed line and the MZI response in red. The grating period is 480 μm and the length is reported to be 10 grating elements. The LPG is formed by using a fusion splicer on the PCF (Crystal Fibre Co., LMA10). The collapsing point is formed by an electric arc. After this local heating, the airholes in the PCF collapse. The collapsing region has a length of 200 μm. The measured fringe spacing is 9.1 nm.

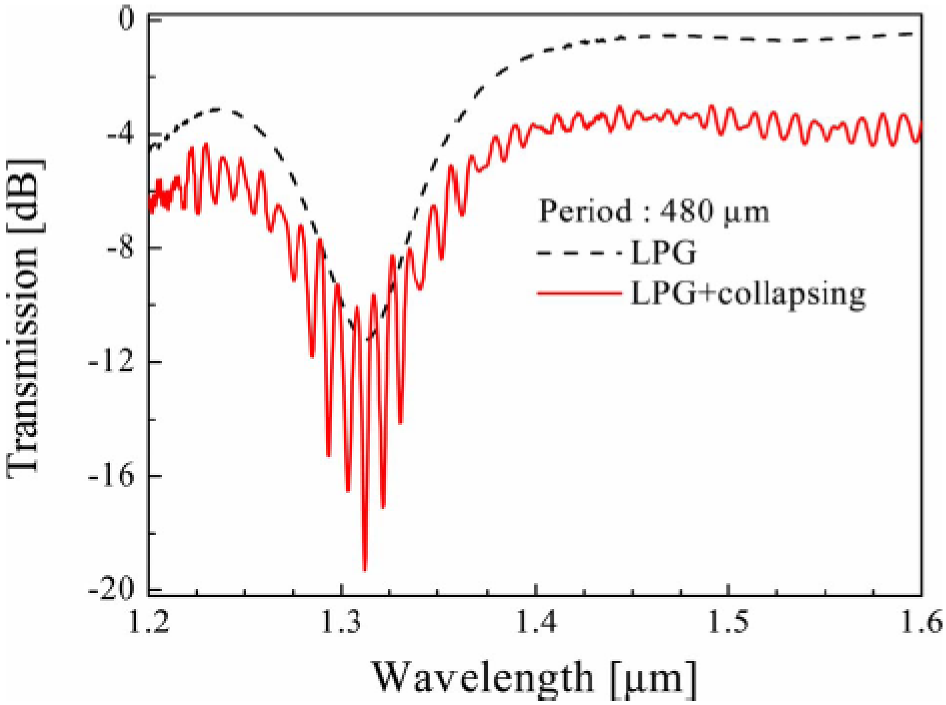

Figure 2.20: Mach-Zehnder interferometer result by Choi *et al*. [22]

2.6 Summary

The identity of ZBLAN fiber is briefly presented. A comparison among the loss performances of the ZBLAN fibers fabricated by different groups is given. Next, a typical procedure of fusion splicing is introduced. The splicing losses are reviewed among the fusion splicing of ZBLAN fibers from different groups. In addition, the operation principles of LPGs and MZIs are described.

Chapter 3 – Fusion Splicing

3.1 Introduction

In this chapter, basic handling of ZBLAN fibers is introduced. Preparations before the fusion splicing such as stripping and cleaving are also presented. The average losses, minimum losses, and fiber strengths of the fusion splices among different types of ZBLAN fibers are discussed.

3.2 Handling

The ZBLAN fibers provided by IRphotonics have a strength above 50 kpsi [8-9]. For this strength, one needs to be very careful with handling the fiber. Any extra pull or bend poses the risk of inducing permanent breaks.

The first step of fusion splicing is stripping, as presented in Fig. 2.8. A piece of fiber is taken and cut (by hand or with a stripper) from a spool. Its length should be long enough to be put on a cleaver and a splicer. For example, around 6 cm is needed for the Ericsson EFC11 cleaver used in this thesis.

IRphotonics ZBLAN fibers are coated with acrylate. Paint remover Circa 1850 is used to facilitate the process of stripping the fiber coating (jacket). It is preferable that an injector is used to contain the paint remover, as it is toxic. The fiber is then inserted in the injector for 10-20 seconds. Then a stripper can remove the fiber coating.

Kimwipes with alcohol are used to clean the stripped part of the fiber. Dust may alter the cleaving and splicing quality. It is important that the fiber remains clean.

3.3 Cleaving

An Ericsson ultrasonic cleaver EFC11 is used for cleaving. Its tension unit is usually set between 85 and 95. There is a trade-off between angle and crack: the higher tension, the flatter angle, but the more cracks, and vice-versa. Fig. 3.1 (a) and (b) are the cleaved fiber inspected from side view and end view respectively, where the tension unit is set at 90.

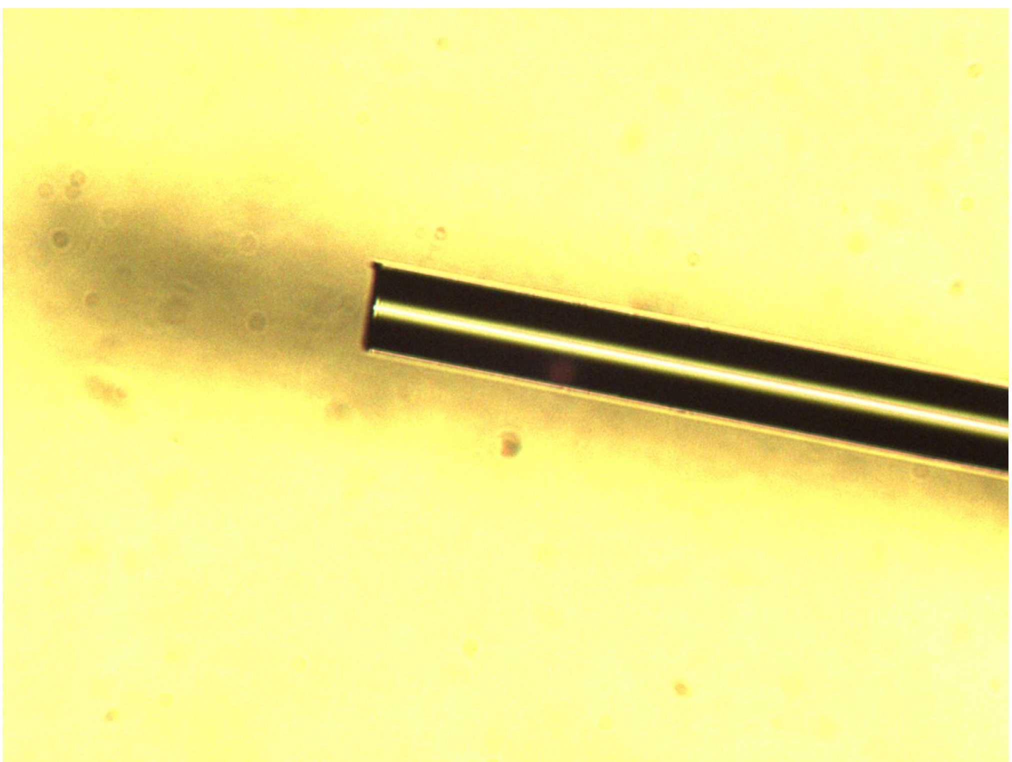

(a)

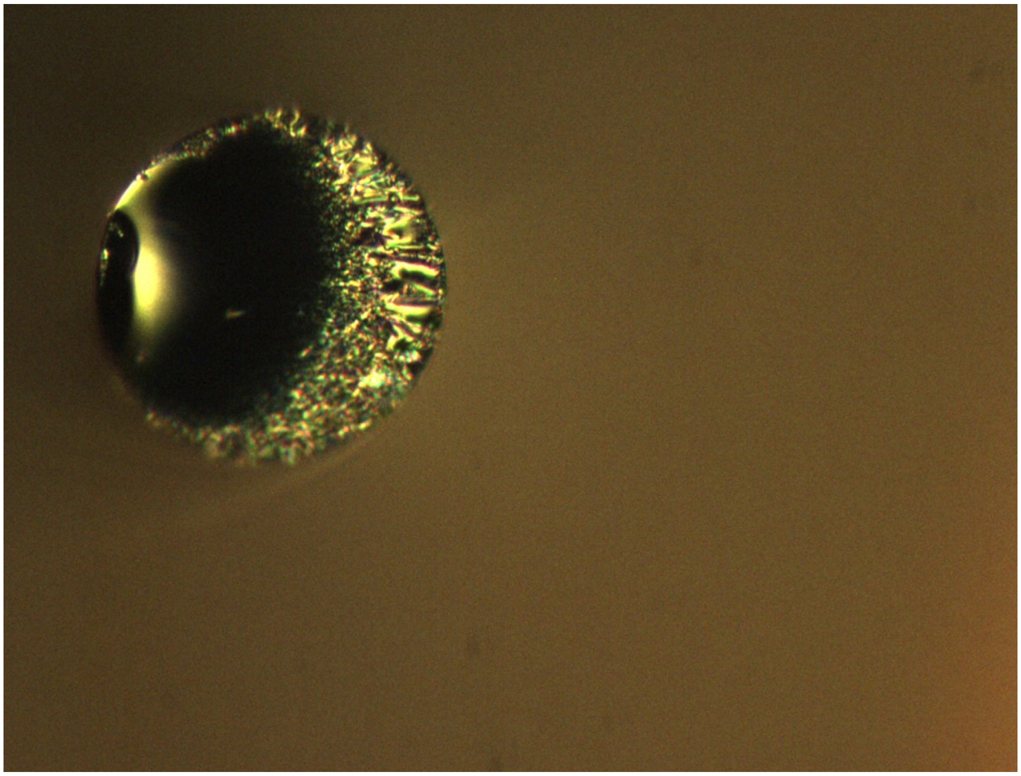

(b)

Figure 3.1: (a) Side view of cleaved ZBLAN fiber (b) End view of cleaved ZBLAN fiber

3.4 Splicing ZBLAN to ZBLAN Fibers

The fiber is placed in V-grooves which are mounted on the splicer. The splicer is a Fujikura FSM-40PM arc fusion splicer. The main parameters that can be controlled on the splicer are arc power, arc duration, and pre-push (the distance between the two tips before the arc).

Fig. 3.2 shows the experimental setup. The source is set at -10 dBm power and 1550 nm wavelength. Pigtail PC connectors are used with MM fiber and bare fiber adapters are used with SM fiber. The spools of MM and SM ZBLAN fiber are put on the sides of the splicer. The transmitted power of the unbroken fiber is measured first at 1550 nm (the power level is denoted as P0), as illustrated in Fig 3.3. The fiber is then separated, stripped and cleaved. After setting the fiber specification and the manual mode, all other parameters are set to off or lowest value (Appendix A). Once the fibers are actively and manually aligned to ensure best transmission, the transmitted power is measured (P1). Next, the arc fusion splicer joins the two fiber tips with specifically designed recipes. The transmitted power is measured again (P2). The loss is calculated by comparing P2 to P1. Usually, the difference between P1 and P0 is within a tolerance of ~0.1 dB because the cleaved tips are not always perfectly flat. Finally, a proof tester (Vytran PTR-200-RPT) is used to measure the fiber strength. Its rotary motors pull the spliced fiber on both ends until it breaks and the instrument records the maximum tension allowed.

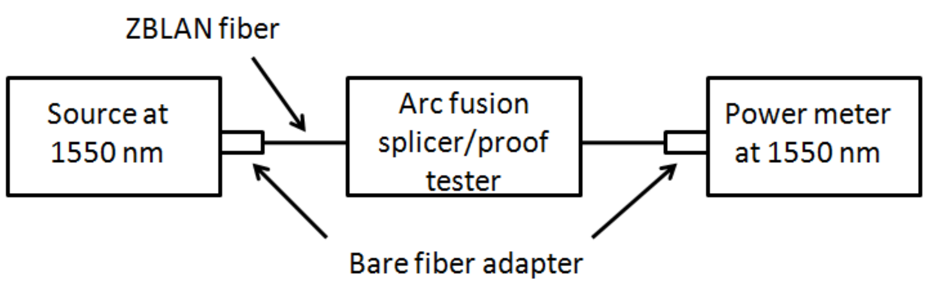

Figure 3.2: Experimental setup for fusion splicing of ZBLAN fibers

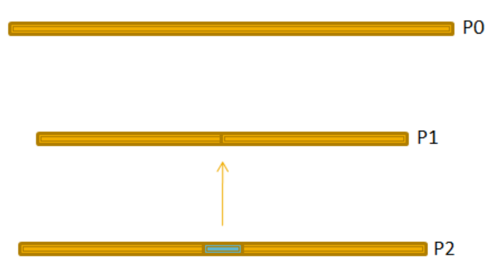

Figure 3.3: Loss measurement

There are two reasons of working under manual mode with this splicer. The arc power in automatic mode seems to be too strong and unstable in the low-temperature regime. Also, the hot push (the reduction of the distance between the two tips during the arc) appears to be so strong or far that it is not reliable for this fragile material. As a result, fusing ZBLAN fiber in this splicer often results in separated tips or core deformations.

Attempts have been made on splicing four types of fiber: MM ZBLAN to MM ZBLAN (MM-MM), SM ZBLAN to SM ZBLAN (SM-SM), SM to MM ZBLAN (SM-MM), SM silica to SM ZBLAN (SiO_2-ZBLAN). The recipes for these splicing are summarized in Table 3.1.

	MM-MM	SM-SM	SM-MM	SiO_2-ZBLAN
Arc Power (bit)	6	-10	20	25
Arc Duration (ms)	30	20	20	20
Pre-Push	Strong	Weak	Weak	Strong

Table 3.1: Recipes for fusion splicing of ZBLAN fibers

3.4.1 Multi-Mode to Multi-Mode Fiber

In the MM-MM splicing, the arc power is set at 6 bits and the arc duration is set at 30 ms. The unit "bit" is proprietary from the splicer company. Thus, the actual temperature or power is unknown. The pre-push is a manual (still motorized) process where the fiber tips are pressed together prior to the fusion. This buckling facilitates the joint of the two softened tips during the fusion. High buckling strength often results in core deformations whereas low buckling strength usually results in weak joint strength. The pre-push of MM-MM is strong because the larger core diameters have better tolerance to the core deformations.

Figs. 3.4 (a)-(c) are from one example of a fusion splice between MM ZBLAN fibers. Fig. 3.4 (a) shows two aligned fiber tips and at same time when P1 of Fig. 3.3 is measured. Fig. 3.4 (b) is the strong pre-push as described in Table 1. Basically, the fibers should be pushed until their cores are near the monitor edge. Fig. 3.4 (c) is a splice with 0.2 dB loss. Fig. 3.5 shows a histogram of 30 splice losses, where the average loss is 0.23 dB, the minimum loss is 0.1 dB. The average strength of the spliced fiber is 36 kpsi out of 5 splices, compared to 50 kpsi of the virgin fiber [8].

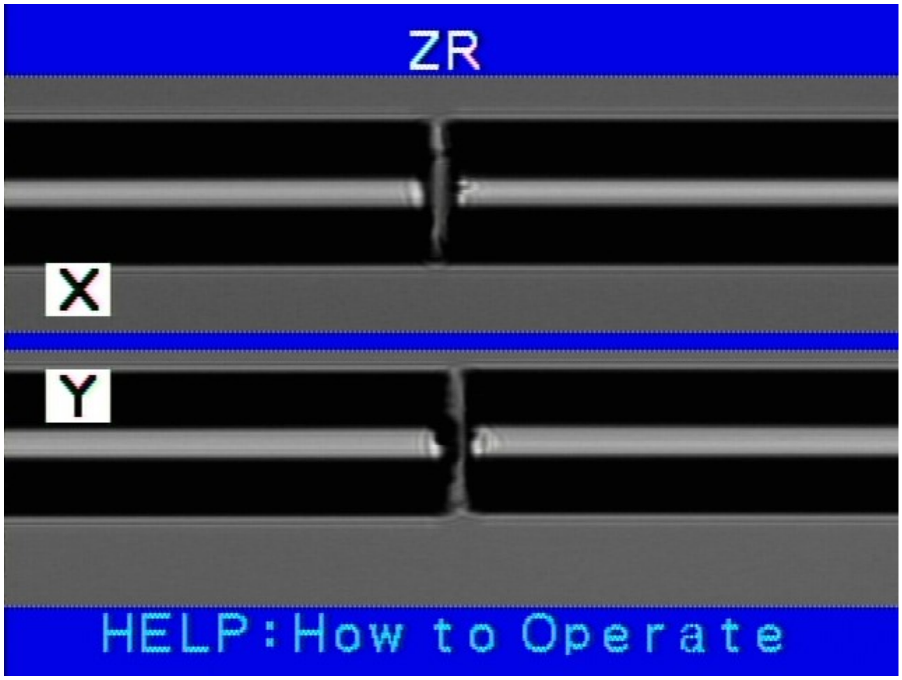

(a)

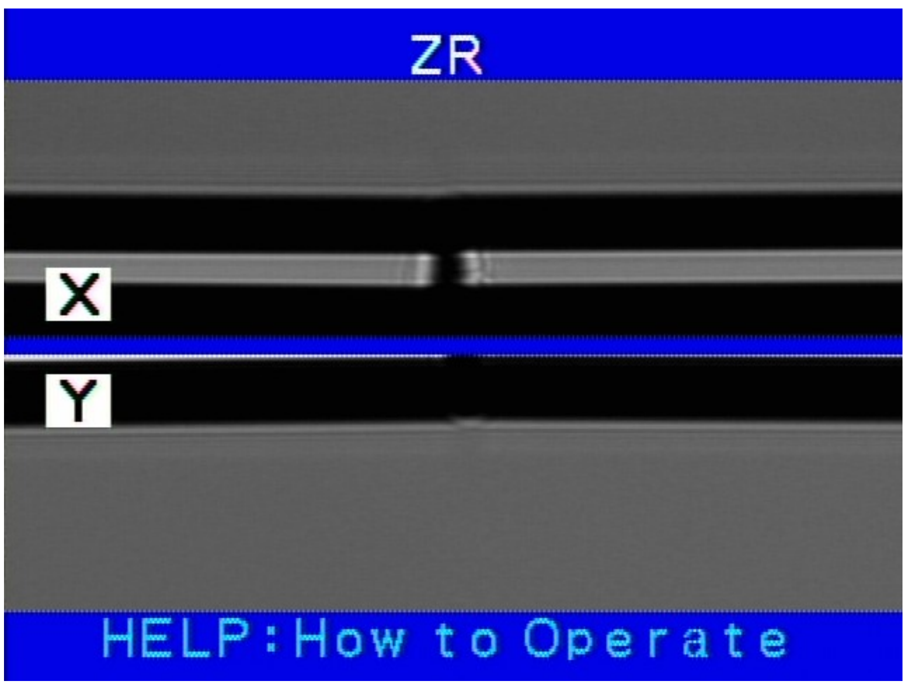

(b)

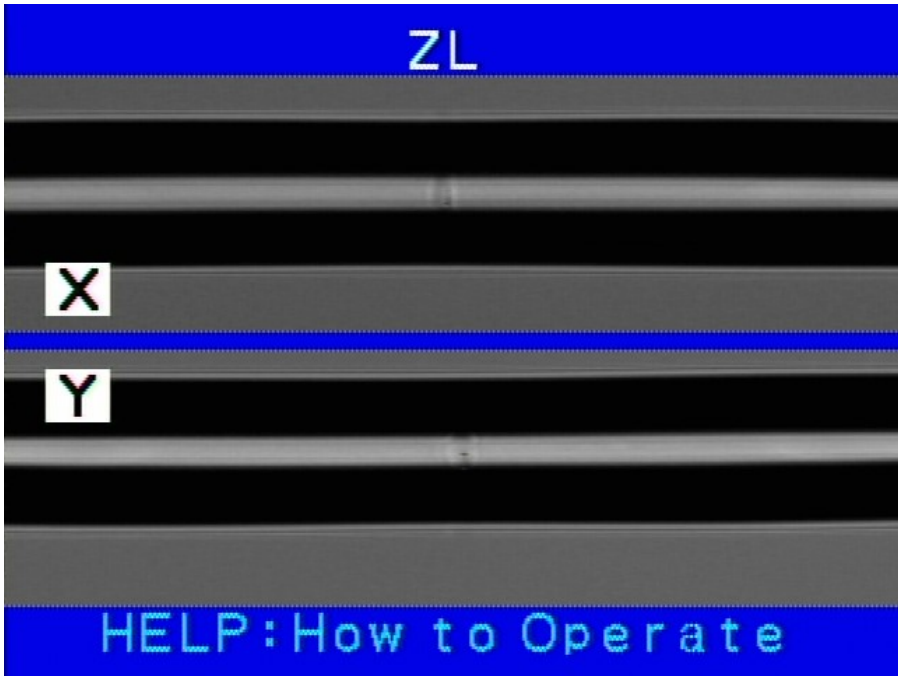

(c)

Figure 3.4 (a) Aligned multi-mode ZBLAN fibers (b) Pre-pushed MM ZBLAN fibers (c) Example of 0.2 dB splice loss from MM ZBLAN fiber splicing

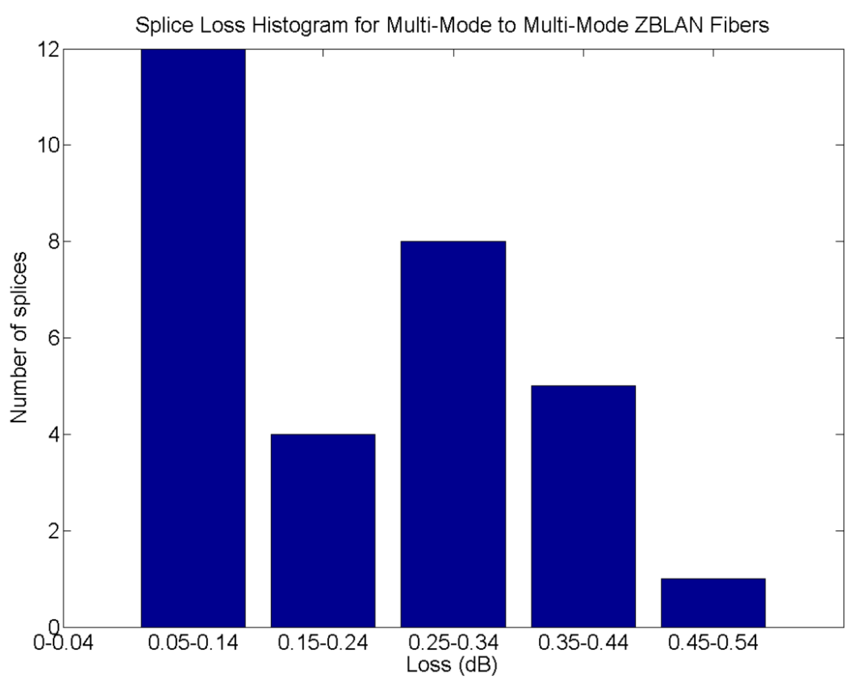

Figure 3.5: Histogram of splice losses from MM ZBLAN fiber splicing

3.4.2 Single-Mode to Single-Mode Fiber

Once the larger core diameter can be spliced, it is reasonable to try the SM ZBLAN fibers which have smaller core diameter. As shown in Table 3.1, the arc power is -10 bits and arc duration is 20 ms. The exposure to heat is reduced because the smaller core is more vulnerable to deformation. Also, one needs to be more careful in alignment. Thus, a weaker pre-push is chosen. The cleaving quality usually results in around 1° of angle detected by the splicer.

Figs. 3.6 (a)-(c) are from one example of a fusion splice between SM ZBLAN fibers. Fig. 3.6 (a) shows two aligned fiber tips and at same time when P1 of Fig. 3.3 is measured. Fig. 3.6 (b) is the weak pre-push as described in Table 1. Basically, the two tips slightly touch each other. Fig. 3.6 (c) is a splice with 0.5 dB loss. Fig. 3.7 shows a histogram of 30 splice losses, where the average loss is 0.31 dB and the minimum loss is 0.1 dB. The average fibre strength after splicing is 8 kpsi (for 5 splices).

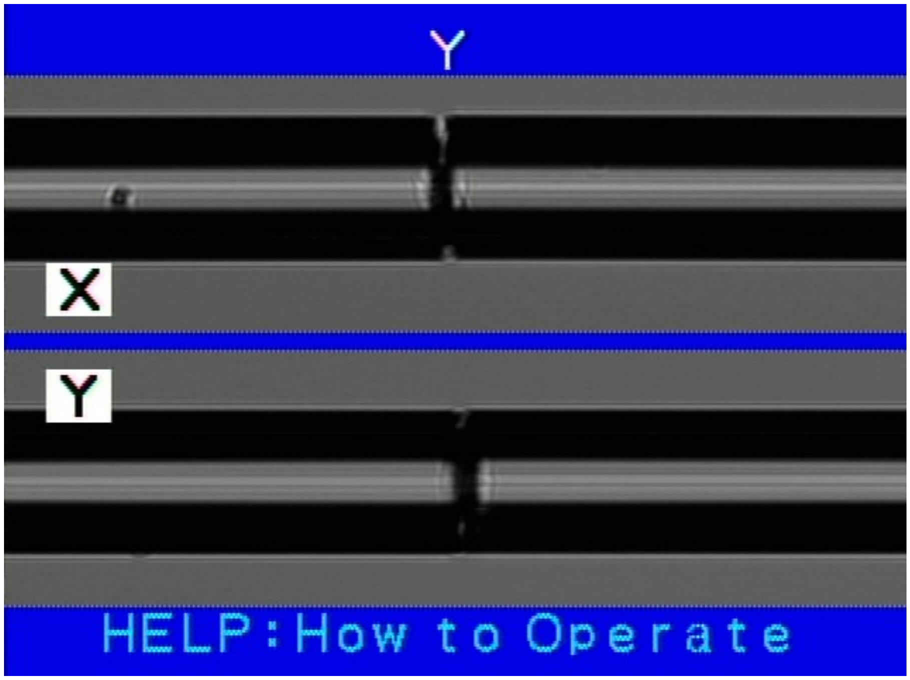

(a)

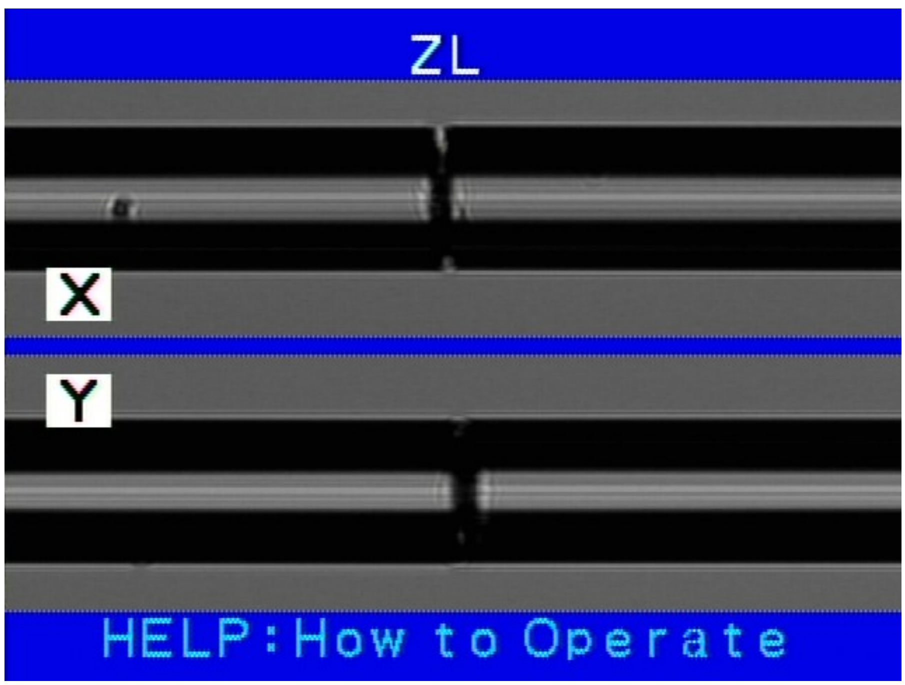

(b)

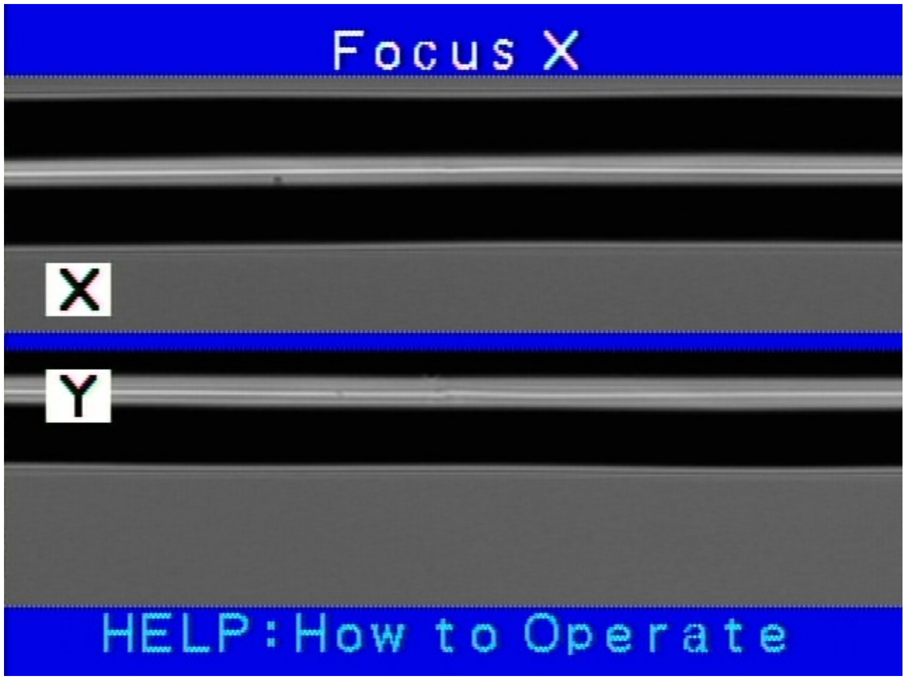

(c)

Figure 3.6 (a) Aligned single-mode ZBLAN fibers (b) Pre-pushed SM ZBLAN fibers (c) Example of 0.5 dB splice loss from SM ZBLAN fiber splicing

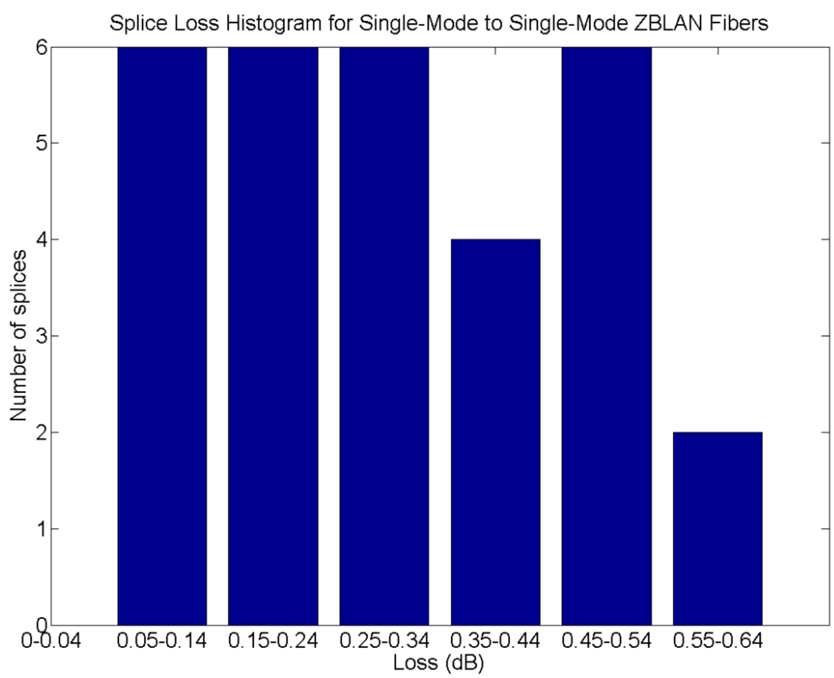

Figure 3.7: Histogram of splice losses from SM ZBLAN fiber splicing

3.4.3 Single-Mode to Multi-Mode Fiber

Splicing SM to MM ZBLAN fibers was also attempted. The light source to measure transmitted power is launched from SM to MM fibers because it is easier to couple light from a smaller core to larger core than the other way around. As for the recipe shown in Table 3.1, the arc power of 20 bits and arc duration of 20 ms are used. The pre-push strength is weak and it is similar to the SM-SM case shown in Fig. 3.6 (b). Fig. 3.8 shows an example of 0.1 dB loss, where MM fiber is on the left side and SM fiber is on the right side. Fig. 3.9 is a histogram of 10 splice losses, where the average loss is 0.3 dB, and the minimum loss is 0.1 dB. For a fiber loss of 0.3 dB, a fiber strength of 41 kpsi was observed. The vertical line in the joint of Fig. 3.8 can be explained by typical observations in low-temperature fusion splicing [11]. It indicates an incomplete joint formed by surface tension. Although the splice can be high-strength and low-loss, it has potentially higher reflectance, which can be further reduced by reheating. Fig. 3.10 shows a silica-based example of the vertical line in low-temperature fusion splicing before (a) and after (b) reheating.

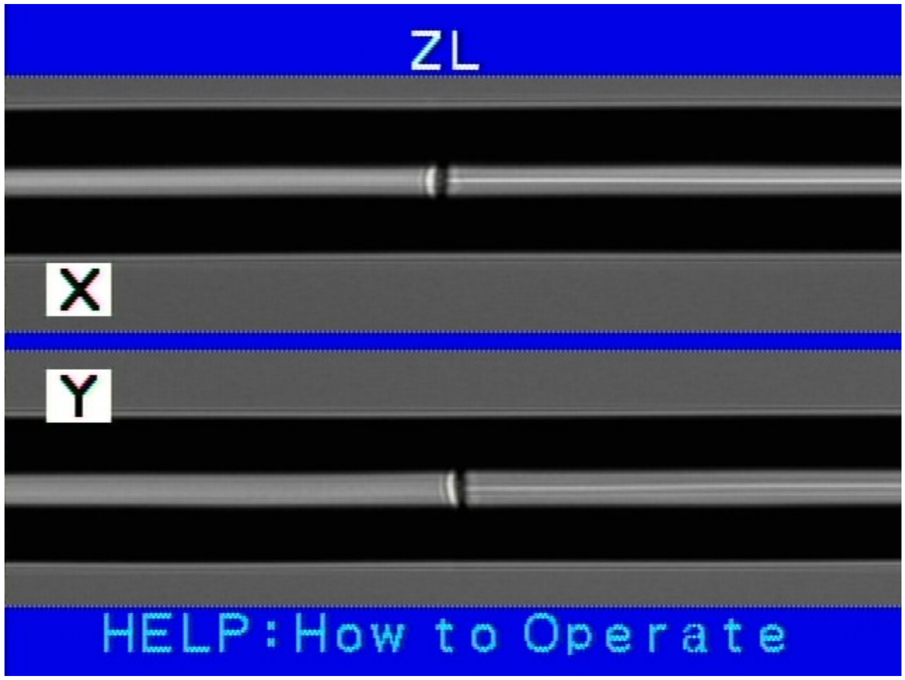

Figure 3.8: Example of 0.1 dB splice loss in SM-MM ZBLAN fiber splicing

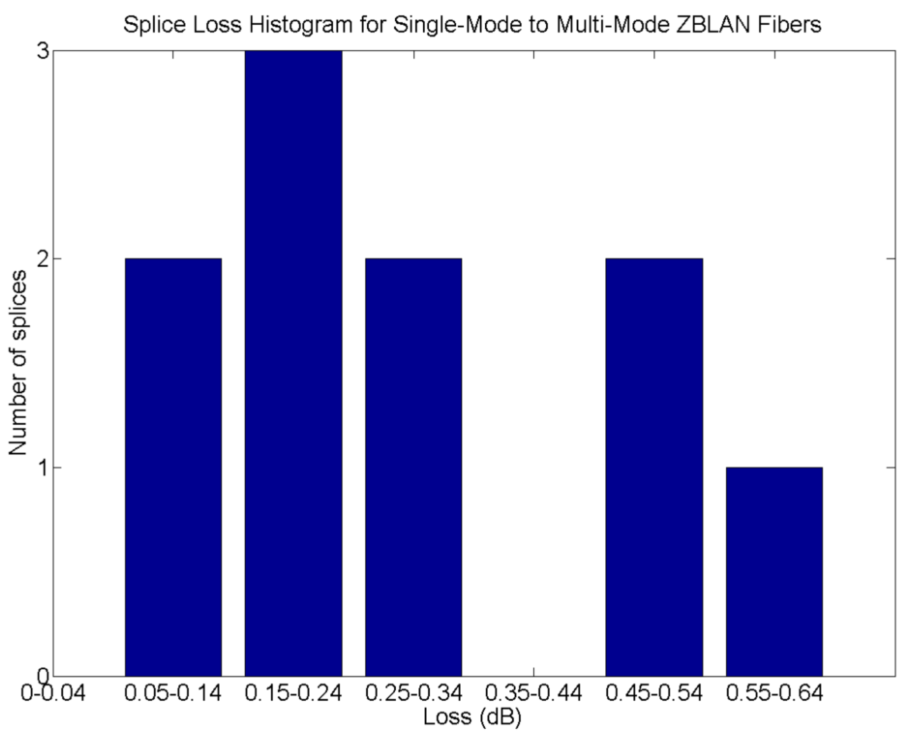

Figure 3.9: Histogram of splice losses in SM-MM ZBLAN fiber splicing

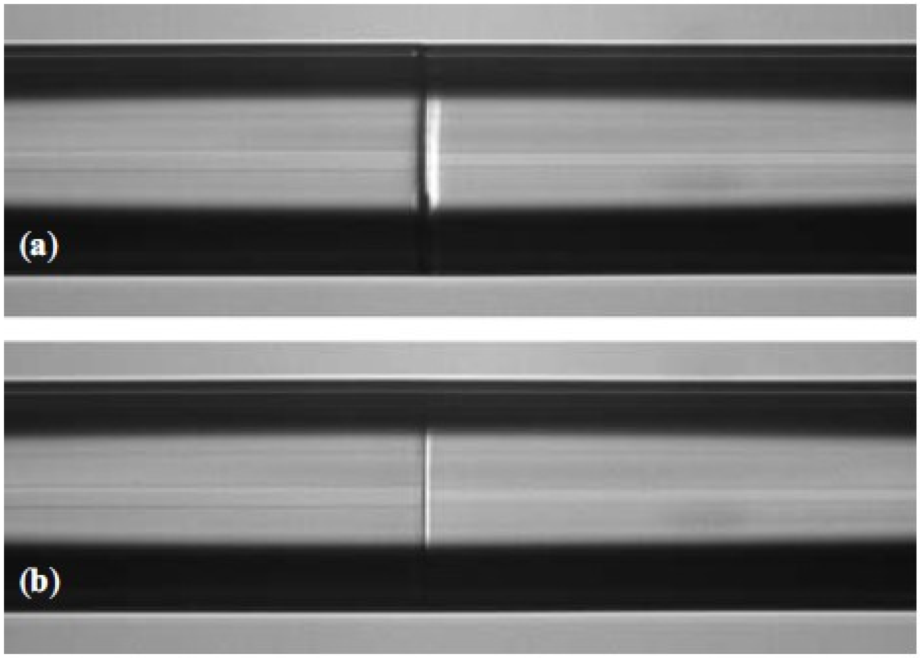

Figure 3.10: Vertical line in low-temperature fusion splicing (a) before and (b) after reheating [11]

3.4.4 ZBLAN Single-Mode to Silica Single-Mode Fiber

Until this point, joint formation occurs between two fibers with similar or same T_g. The challenge of splicing a ZBLAN fiber onto a silica fiber is that the two fibers have different T_g. As shown in Table 1.1, The T_g of ZBLAN is 259 °C and T_g of silica is 1175 °C. If the temperature is as low as that used in the previous splicings, then only the ZBLAN side is softened. On the other hand, if the temperature is high enough to soften the silica side, then the ZBLAN side is damaged. There are few approaches to this type of splicing. One way is to shift the heat zone appropriately towards the silica side. As a result, the two sides encounter different temperatures where the side with higher T_g is closer to the arc center. Fig. 3.11 shows an attempt of splicing ZBLAN fiber to silica fiber. The

ZBLAN side (left) is softened and “glued” onto the silica side (right). The recipe from Table 1 has 25 bit arc power, 20 ms arc duration, and strong pre-push strength which is similar to the MM-MM case in Fig. 3.4 (b). Significant core deformation is observed here. Therefore, this splicing technique has not been perfected yet. It would need a specialized heating profile (such as shifting the fusion center towards the silica fiber), pushing techniques, or intermediate media such as a material with an appropriate T_g to improve this splicing.

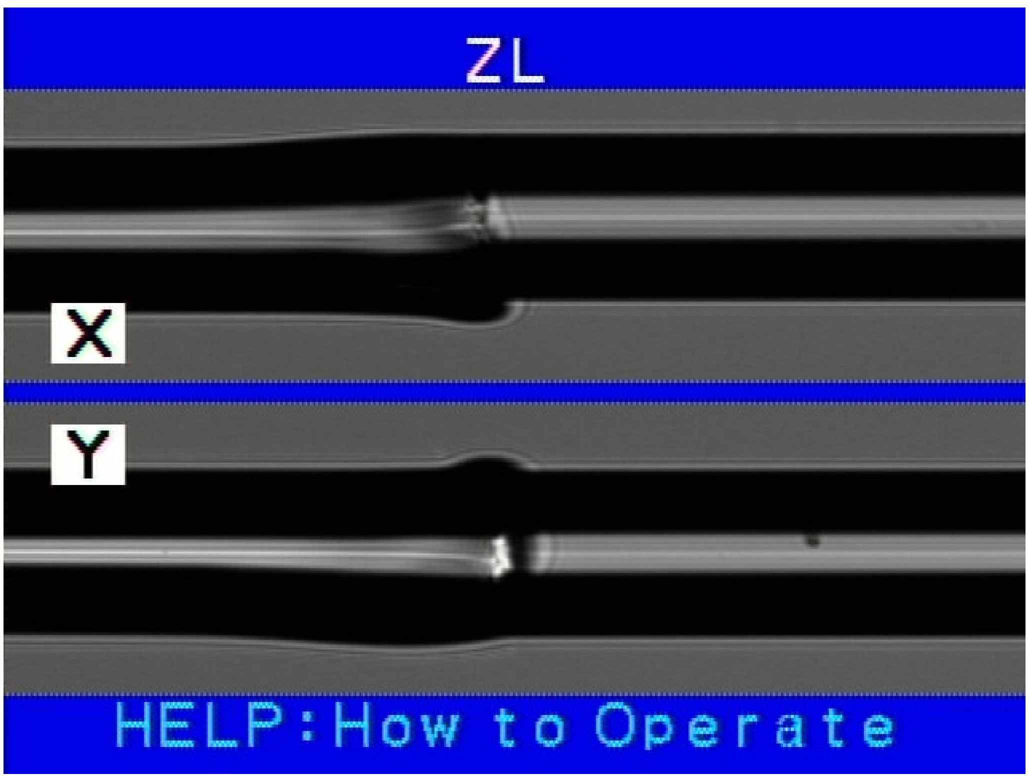

Figure 3.11: Example of fusion splicing between SM ZBLAN fiber and SM silica fiber

3.5 Summary

In this chapter, the experiments of 4 types of arc fusion splicing involving ZBLAN fibers are described. Table 3.2 summarizes the experimental results. For the MM-MM ZBLAN fusion splicing, the average loss is 0.23 dB, the minimum loss is 0.1 dB, and the fiber strength is 36 kpsi. For the SM-SM ZBLAN fusion splicing, the average loss is 0.31 dB, the minimum loss is 0.1 dB, and the fiber strength is 8 kpsi. For the SM-MM ZBLAN fusion splicing, the average loss is 0.3 dB, minimum loss is 0.1 dB, and the fiber strength is 41 kpsi. Currently, the measurements for the splicing between silica and ZBLAN are not available. However, the formation of a joint is encouraging.

	Number of Trials	Average Loss (dB)	Variance	Minimum Loss (dB)	Strength (kpsi)
MM-MM	30	0.23	0.016	0.1	36
SM-SM	30	0.31	0.026	0.1	8
SM-MM	10	0.3	0.031	0.1	41

Table 3.2: Summarized results for ZBLAN fusion splicing

Chapter 4 – Mechanically-Induced Long-Period Gratings in ZBLAN Fibers

4.1 Introduction

In this chapter, the fabrication and the setup of mechanically-induced LPGs are described. Furthermore, the spectral response is measured in the O- and C-bands. Finally, the measured responses are compared to simulations.

4.2 Method

The approach taken to make LPGs on ZBLAN fibers is by pressing set screws (threaded rods) on the coated fiber. Again, one needs to be careful with applying forces on an already fragile material. Prototypes are developed to achieve this mechanical effect. Two of them are presented in Fig. 4.1 (a) (Clamp 1) and Fig. 4.1 (b) (Clamp 2). Clamp 1 consists of a one-axis clamp, a threaded rod, two rods used for confinement, and a V-groove. Clamp 2 consists of a one-axis clamp, a threaded rod, and an “L-shape” formed by two plates. The L-shape confines the rod on the side and on the bottom part. Tape is used to better confine the fiber and to add protection against the screw.

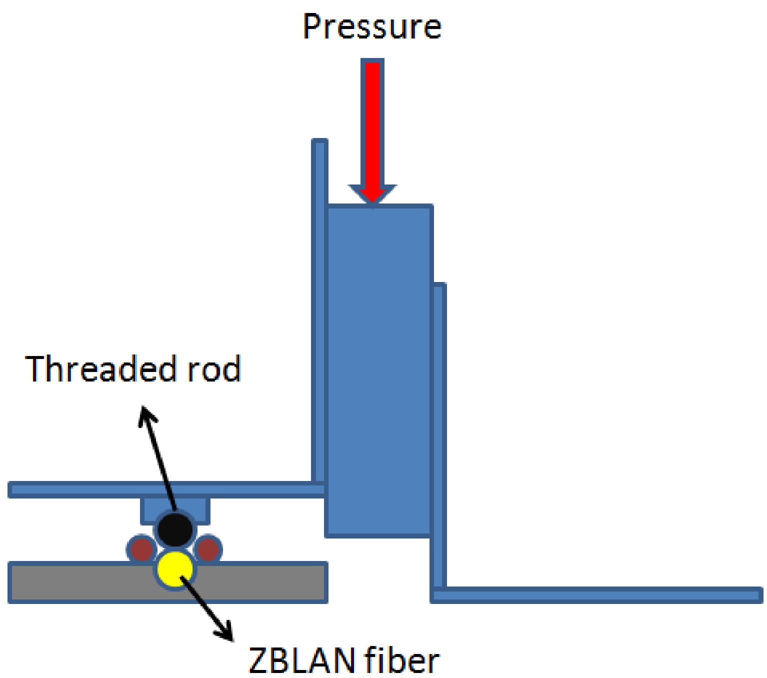

(a)

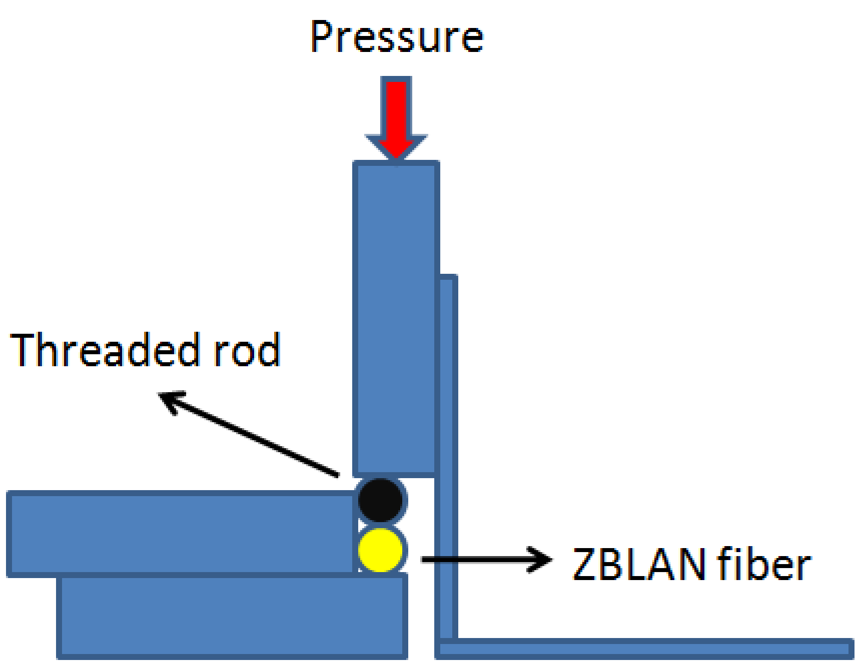

(b)

Figure 4.1 (a) "Clamp 1" v-grooved clamp for mechanically induced LPG (b) "Clamp 2" L-shaped clamp for mechanically induced LPG

Fig. 4.2 illustrates the experimental setup to fabricate and measure LPGs in ZBLAN fibers. An unpolarized BBS is connected to the single-mode ZBLAN fiber via a bare-fiber adapter. The sources used were a semiconductor optical amplifier (SOA) operating at 1310 nm and an erbium-doped fiber amplifier (EDFA) at 1550 nm. A SM ZBLAN fiber, with a core diameter of 9 μm, a cladding diameter of 125 μm, a core refractive index of 1.488, and an NA of 0.17 is used [9]. Note that the fiber works in the MM regime in O- and C-bands. A section of the fiber rests in a V-groove (Fig. 4.1a) or a flat plate (Fig. 4.1b) while a threaded steel rod is placed onto it. The ends of the fiber are taut and carefully positioned to minimize microbends and twists to avoid inducing additional birefringence. The protective fiber coating is kept. A clamp is used to press the threaded steel rod and can be adjusted to different applied pressures. The resulting transmission spectrum is displayed on an optical spectrum analyzer (OSA) with resolution of 0.05 nm.

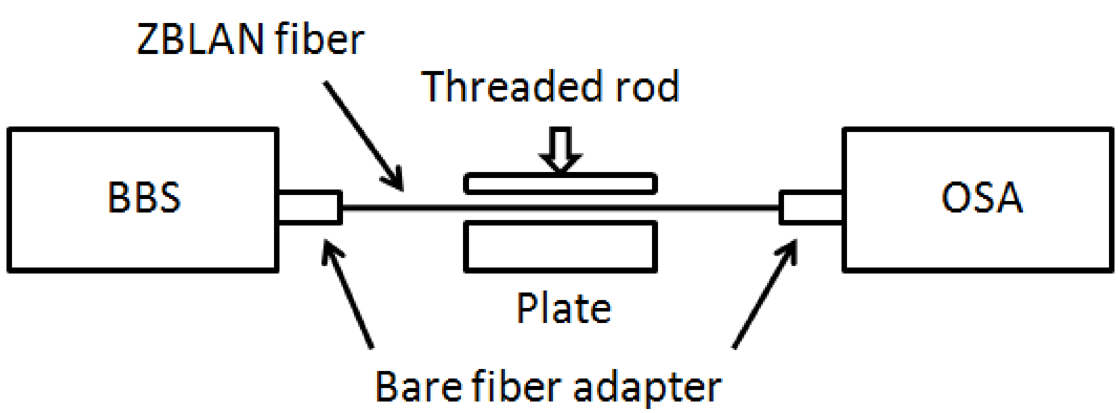

Figure 4.2: Experimental setup for mechanically induced LPG on ZBLAN fibers

4.3 Pressure Dependence

Two LPG structures are developed in this thesis. LPG_1 consists of a screw with a length of 32 mm, grating period Λ = 1.27 mm, and is used only in Clamp 1. LPG_2 consists of a screw with a length of 25.4 mm, grating period Λ = 0.71 mm, and is used only in Clamp 2. The threaded rods are made under the Unified Thread Standard (UTS).

Fig. 4.3 shows a typical response of LPG_2 (Λ = 0.71 mm) over the O-band (a) and C-band (b) as a function of increasing pressure. The applied pressure increases from P0 to P5 and is released back to $P0_2$. Three stopbands are observed: (1) ~9 dB deep around 1260 nm, (2) ~11 dB deep around 1320 nm, and (3) ~20 dB deep around 1560 nm. The wavelength region between the two bands is omitted because the BBS does not extend to that range. After the release of pressure ($P0_2$), the spectral transmissivity returns to the initial shape (P0). Thus, an LPG made by this mechanical approach is reversible.

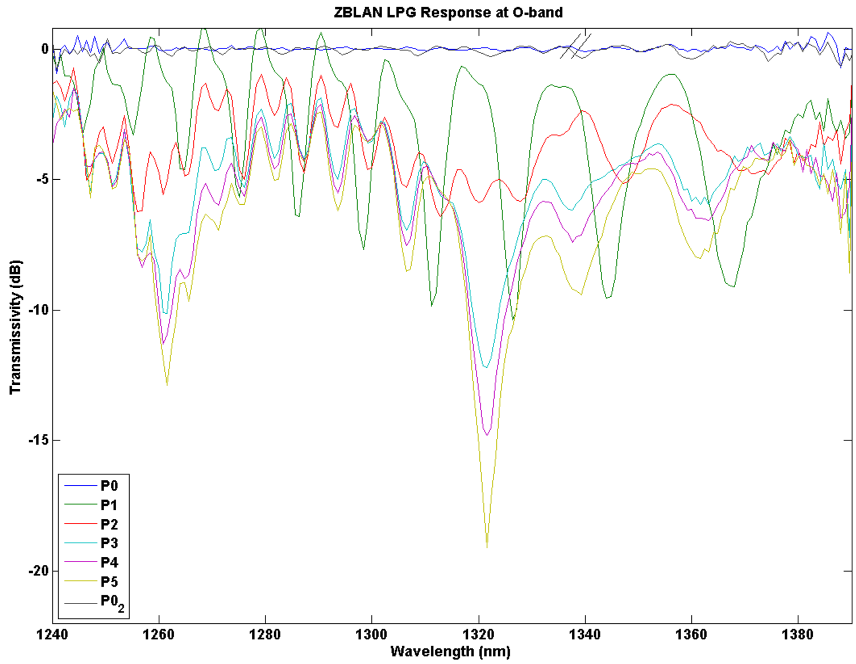

(a)

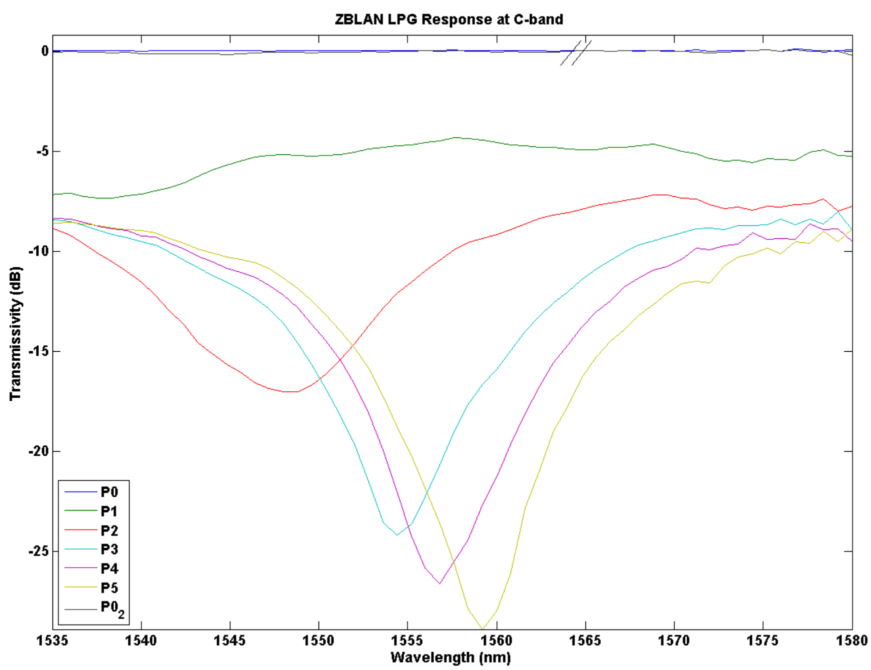

(b)

Figure 4.3: ZBLAN LPG response in (a) O-band and (b) C-band for LPG_1 for different applied pressure

The reason that the peak wavelength shifts as the pressure increases may be attributed to pressure induced changes in refractive indices [40-41]. A similar effect is found for photoinduced LPGs, where the effective refractive index increases for longer UV exposure. Fig. 4.4 shows an example of wavelength shift in photoinduced LPGs as a function of exposure time [15].

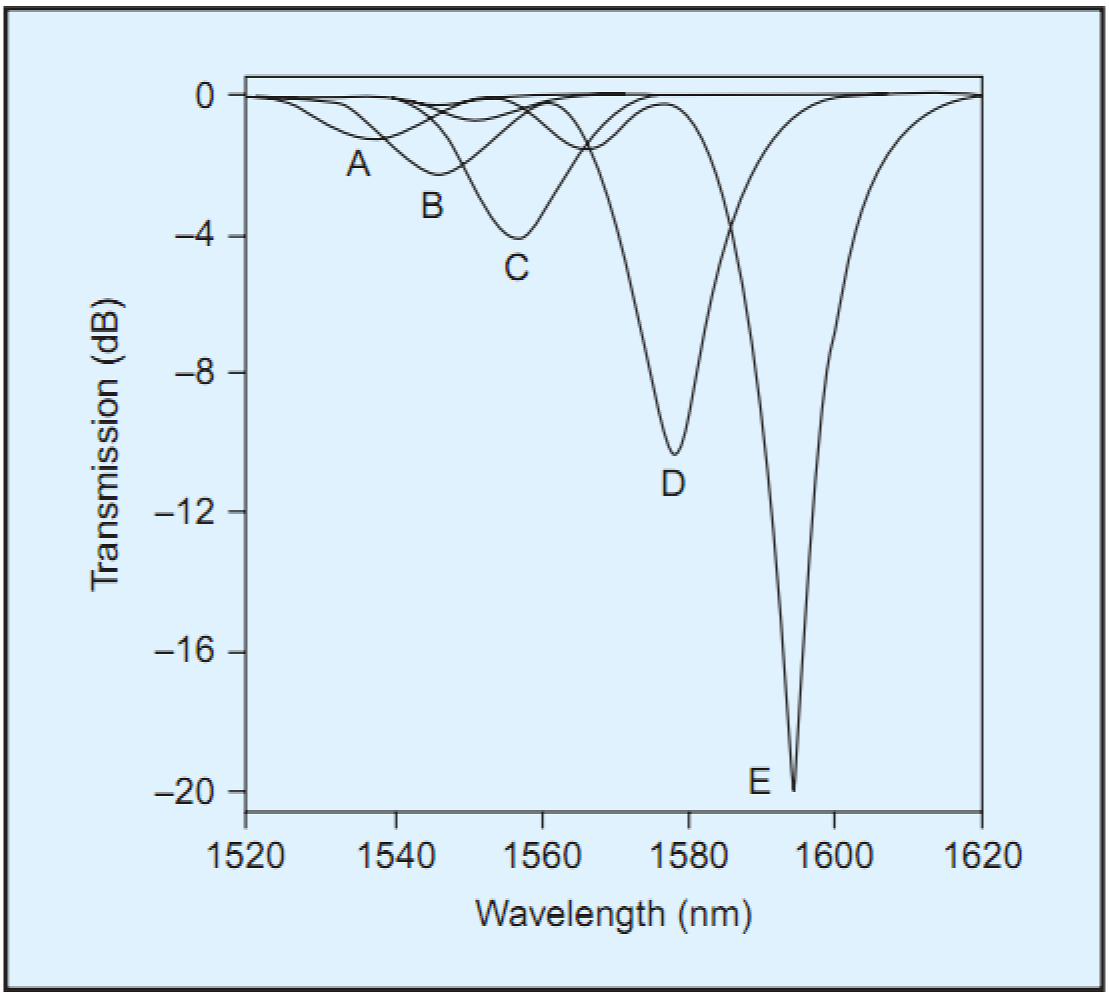

Figure 4.4: Wavelength shift during photoinduced growth of LPG. A: 1 min, B: 2 min, C: 3 min, D: 4 min, E: 5 min [15]

One way to quantify the applied pressure is by measuring the downward displacement of the clamp, i.e., the distance of the plate above the fiber has traveled down. Fig. 4.5 (a) shows the evolution of the LPG_2 response as a function of displacement. 6 displacements have been recorded: 0 cm, 1 cm, 1.24 cm, 1.28 cm, 1.52 cm, and 0 cm again. The peak stopband appears at a displacement of 1.52 cm with approximately 8 dB depth at around 1531 nm. The insertion loss may be attributed to the pressure-induced attenuation. It is experimentally tested that if a unthreaded rod is pressed on the fiber, the insertion loss will increase as the transmissvity baseline goes down and no stopband appears. The wavelength shift may be due to the pressure-induced index changes. Figs. 4.5 (b) and (c) show the wavelength shift and the insertion loss as a function of clamp displacement, respectively.

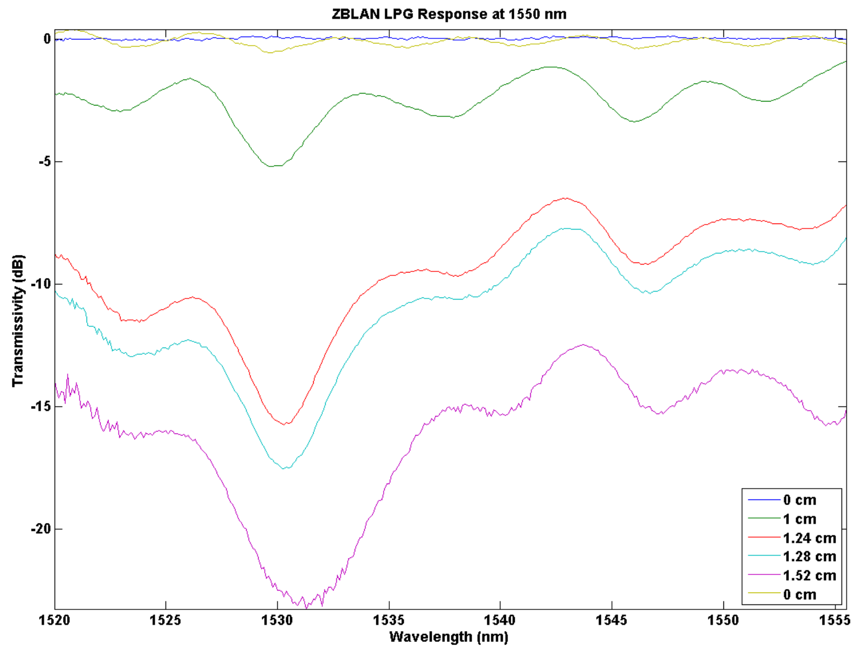
ZBLAN LPG Response at 1550 nm
Transmissivity (dB)
Wavelength (nm)
0
-5
-10
-15
-20
1520
1525
1530
1535
1540
1545
1550
1555
0 cm
1 cm
1.24 cm
1.28 cm
1.52 cm
0 cm

(a)

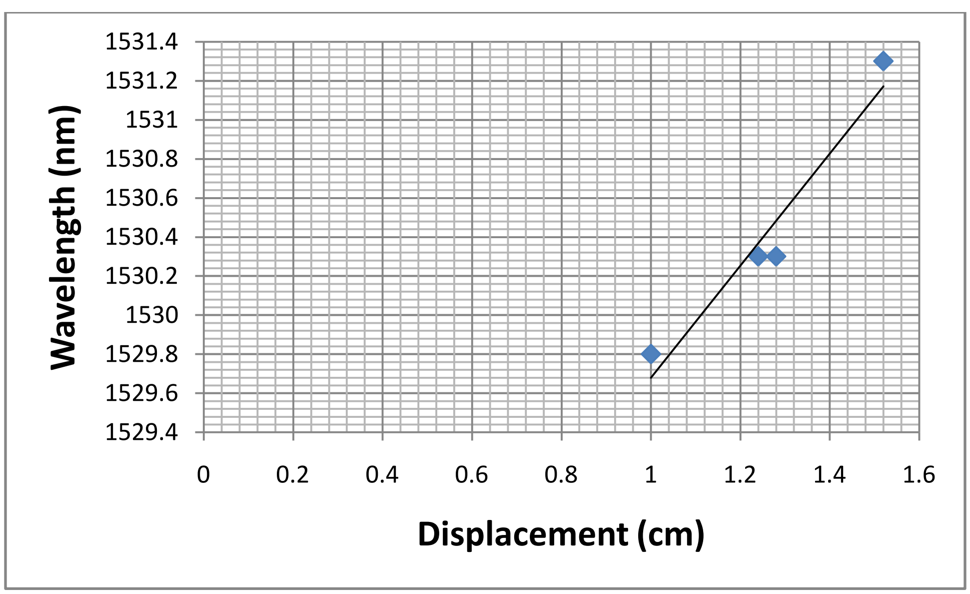
Wavelength (nm)
Displacement (cm)
1531.4
1531.2
1531
1530.8
1530.6
1530.4
1530.2
1530
1529.8
1529.6
1529.4
0
0.2
0.4
0.6
0.8
1
1.2
1.4
1.6

(b)

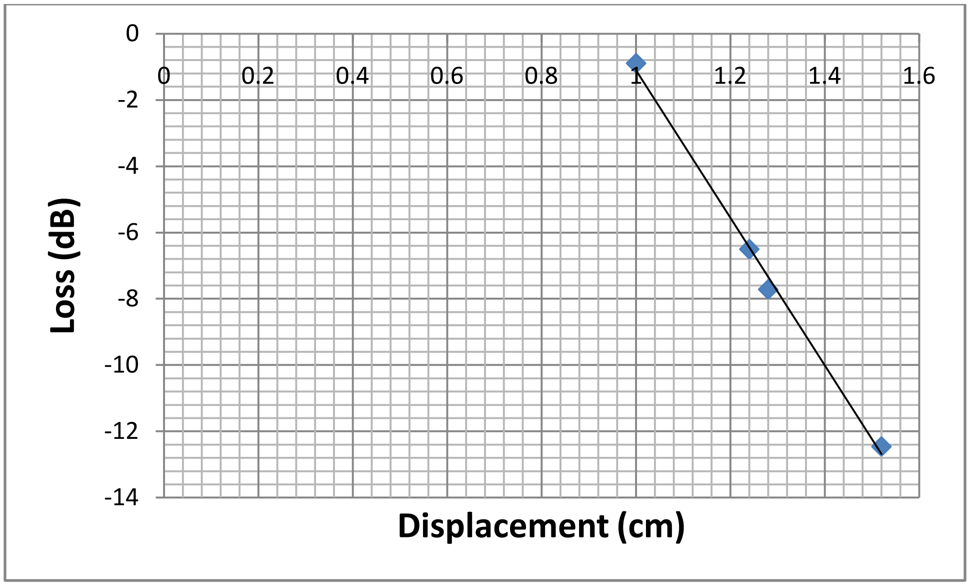

(c)

Figure 4.5: (a) ZBLAN LPG response as a function of displacement of the clamp (b) Wavelength shift as a function of displacement (c) Insertion loss as a function of displacement

4.3.1 Response in the C-band

In the C-band, there are results from the two grating structures. Fig. 4.6 (a) shows the result obtained from LPG_1. The stopband near 1525 nm is 6.5 dB deep with 6 dB insertion loss. Fig. 4.6 (b) shows the result obtained from LPG_2. It shows the evolution of a single transmission notch as a function of pressure. The notch depth deepens as the pressure is increased. The deepest stopband near 1550 nm is 16 dB deep with 9 dB insertion loss.

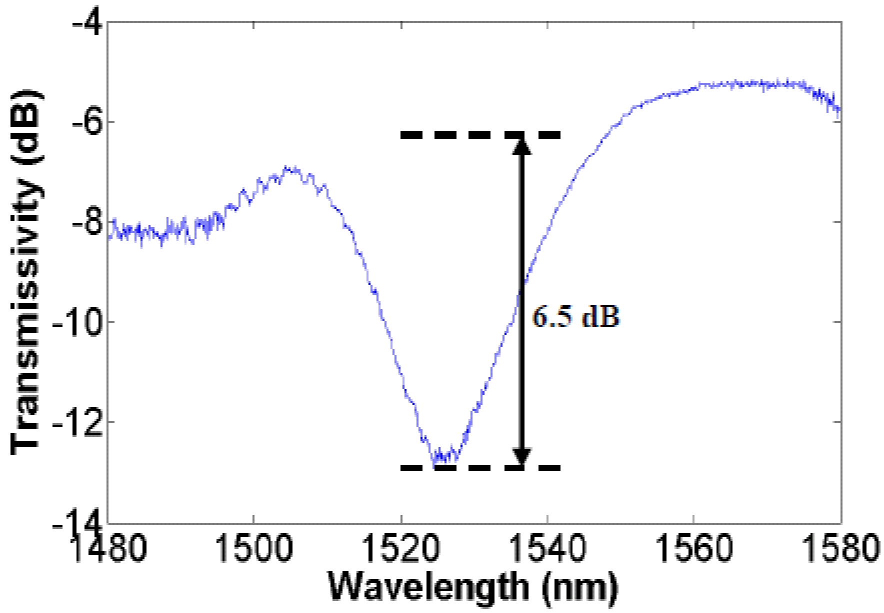

(a)

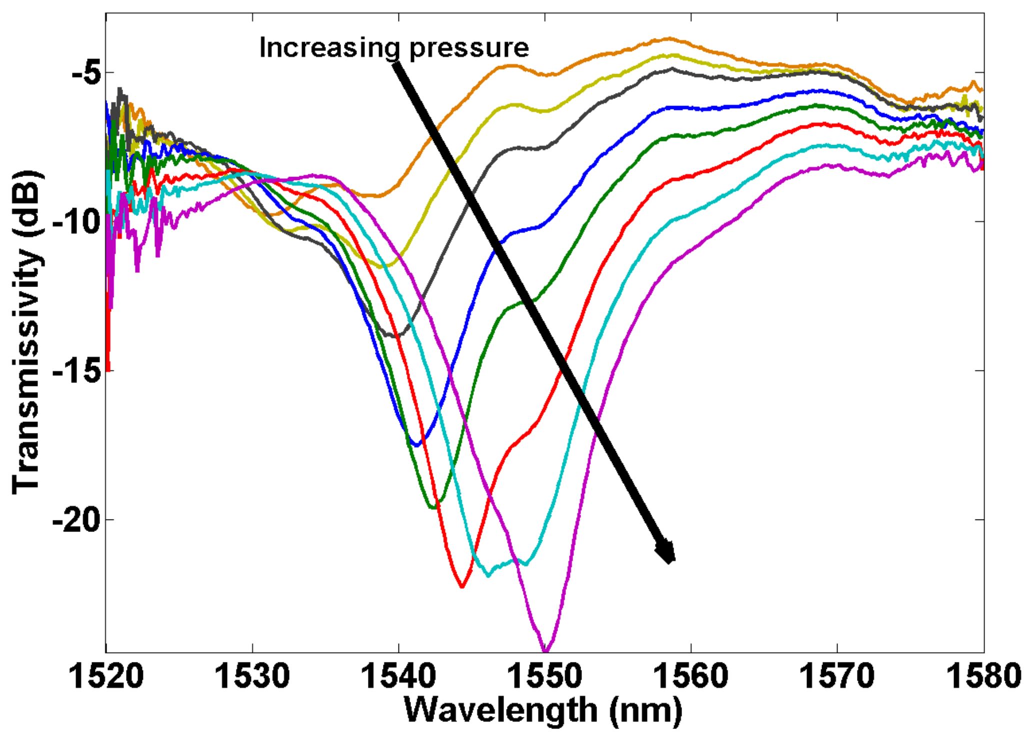

(b)

Figure 4.6: Measured spectral responses of (a) LPG_1 and (b) LPG_2 in the C-band

4.3.2 Response in the O-band

In the O-band, there are also results from the two grating structures. Fig. 4.7 (a) shows the result obtained from LPG_1. The stopband near 1365 nm is 6 dB deep with 1 dB insertion loss. Fig. 4.7 (b) shows the result obtained from LPG_2. At maximum pressure, there are two stopbands: one near 1335 nm is 16 dB deep with 9 dB insertion loss while the second stopband near 1270 nm is 17 dB deep with 8 dB insertion loss.

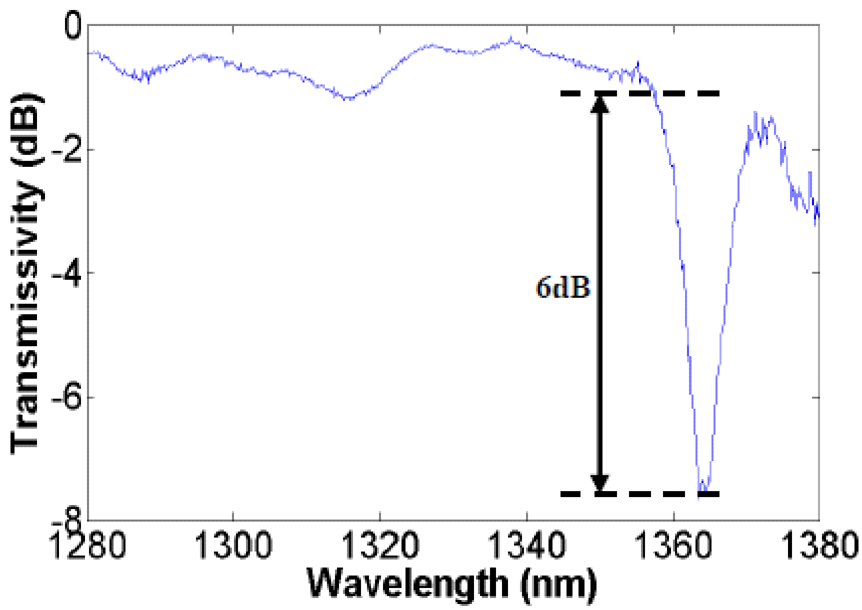

(a)

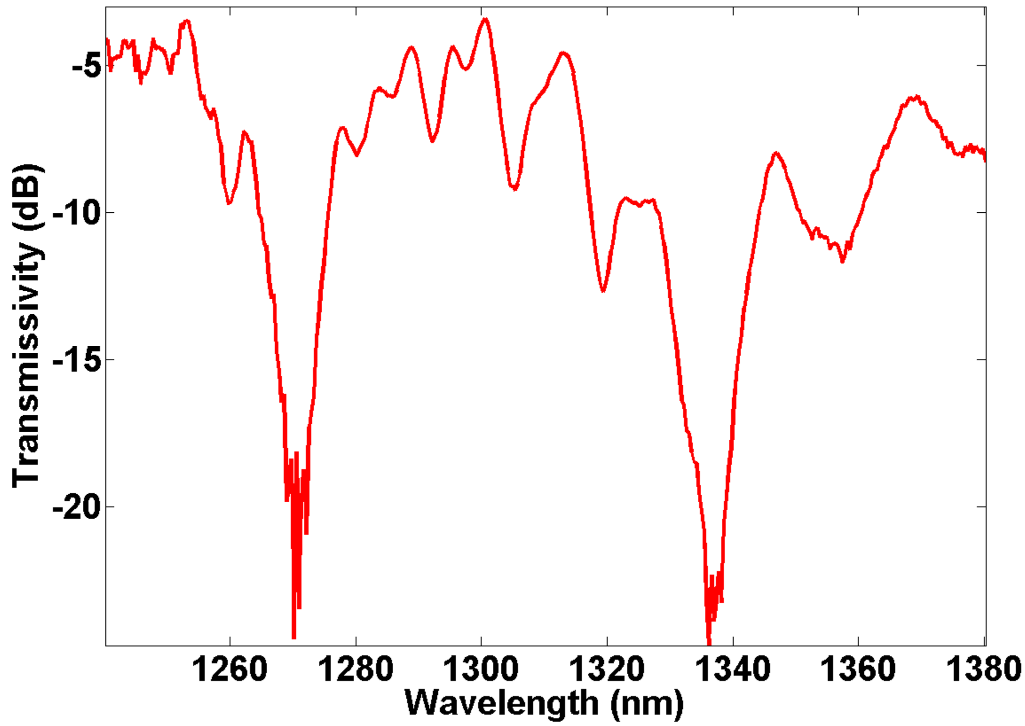

(b)

Figure 4.7: Measured spectral responses of (a) LPG_1 and (b) LPG_2 in the O-band

4.4 Simulation

By using the F-matrix method, an LPG is simulated (Appendix B) in order to compare with that of Fig. 4.6 (b) [42]. Fig. 4.8 compares the simulated and measured LPG_2 in the C-band.

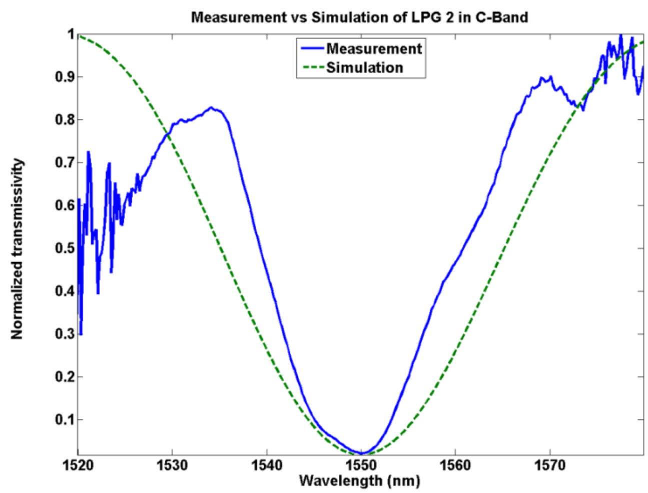

Figure 4.8: Comparison between the simulated and measured LPG in C-band (LPG_2)

One significant difference is the insertion loss introduced by pressing the fiber. The fact that the measured notch is narrower than the simulated one may be attributed to the triangular shape of the peaks in a threaded rod. As a result, the grating period may reduce as the threaded rod penetrates into the fiber. The parameters used in the simulation are summarized in Table 4.1.

Grating Length (mm)	Grating Period (mm)	Peak (nm)	Overlap Integral	Amplitude of perturbation
25.4	0.639	1550	0.62	$1.5848 \cdot 10^{-4}$

Table 4.1: The parameters used to simulate the LPG_2 in C-band

Using the same parameters, the LPG response at the O-band is also simulated and compared to measurements, see Fig. 4.9. The differences could be from the insertion losses and pressure induced birefringence.

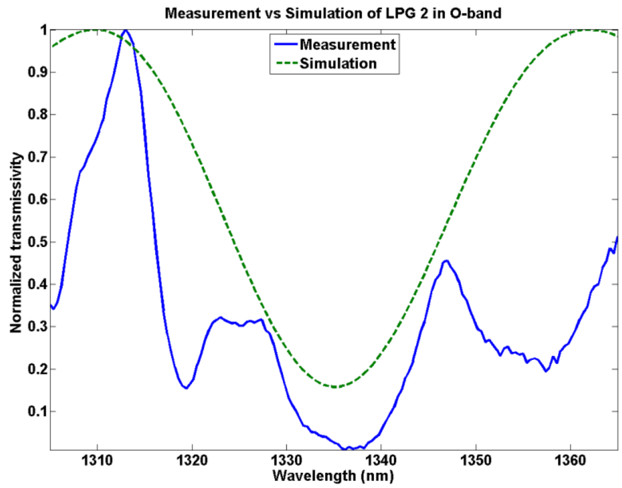

(a)

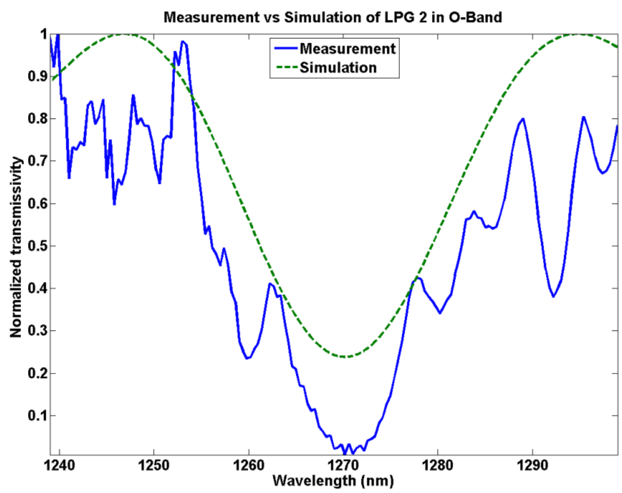

(b)

Figure 4.9: Comparison between the simulated and measured LPG_2 in O-band (a) 1335 nm (b) 1270 nm

4.5 Summary

In this section, LPGs are mechanically induced on ZBLAN fibers by pressing threaded rods on them. The dependence of pressure is investigated. The results are summarized as follows. With LPG_1, a 6.5 dB notch is observed at 1525 nm with a 6 dB insertion loss. A 6 dB notch is observed at 1365 nm with a 1 dB insertion loss. With LPG_2, a 16 dB notch appears at 1550 nm with a 9 dB insertion loss. Also, a 16 dB notch appears at 1335 nm with a 9 dB insertion loss and a 17 dB notch appears at 1335 nm with a 8 dB insertion loss. The comparisons with the simulations based on the F-matrix method are presented and some discussions on the differences are given. They match reasonably well but the differences due to the insertion losses and pressure induced birefringence are present.

Chapter 5 - Mach Zehnder Interferometer

After having success with mechanically induced LPGs on ZBLAN fibers, it is reasonable to try adding a second one in a cascaded structure in order to make an interferometer. Fig. 5.1 shows the experimental setup where two L-shape clamps (clamp 2) are used to induce 2 separated LPGs. An EDFA at 1550 nm is used as the BBS. Two bare fiber adapters are used to connect the ZBLAN fiber to the BBS and the OSA. The fiber in use is SM ZBLAN fiber with 9 μm core diameter, 125 μm cladding diameter, and an NA of 0.17. Therefore, the fiber works in the MM regime in the C-band (Appendix C). Two threaded rods with the same grating specification (period of 0.71 mm and length of 25.4 mm) are used in order to have LPGs that overlap spectrally around 1530 nm. A length of bare fiber L separates the two gratings. At the end, an OSA (resolution 0.05 nm) is used to record the spectral response.

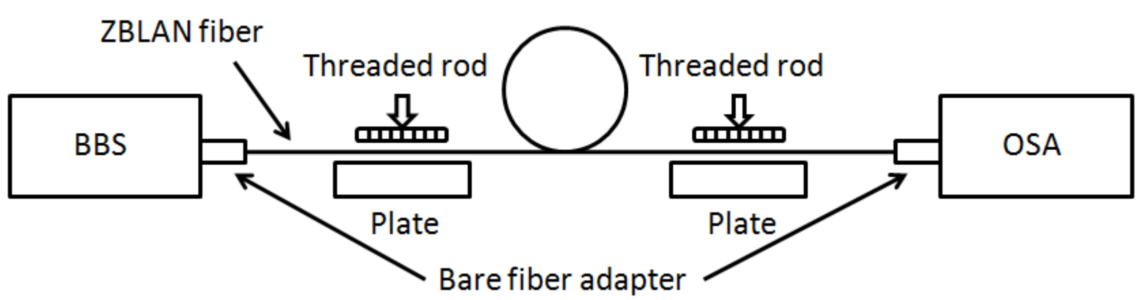

Figure 5.1: Experimental Setup of Cascaded LPGs

To create the spectral overlap of the two LPGs, the alignment between the threaded rod and the fiber of each LPG is adjusted iteratively. The overlap can be inferred by having each clamp pressed one at a time. Since the mechanically induced LPG is reversible and repeatable, each LPG response can be observed individually and then combined when the respective clamp displacements create the spectrally overlapped responses. As shown in Fig. 4.5, the wavelength shift and insertion loss depend on pressure. Sometimes, an overlap is achieved by pressing harder where the wavelength range of one LPG shifts to that of the other LPG. As a result, some results have higher insertion loss, see Fig. 5.2 (a) for example. In this case, the ideal strength of 3 dB per LPG for a dual-LPG based MZI might not be obtained. Less ideal MZIs based on cascaded LPGs are obtained usually due to an incomplete overlap or a notch too far away from 3 dB.

By varying the separation length between the centers of the two gratings, the fringe spacing should change accordingly. In principle, the spacing should be inversely proportional to the separation [24]. The fringe spacing is given by:

$$S \approx \frac{\lambda^2}{\Delta m L} \tag{5.1}$$

where $\boldsymbol{\lambda}$ is the center wavelength, $\boldsymbol{\Delta m}$ is the effective group index difference, and $\boldsymbol{L}$ is the center-to-center separation between the gratings. The results are summarized in Fig 5.2: for $\boldsymbol{L}$ = 133 cm, $\boldsymbol{S}$ = 2.17 cm; for $\boldsymbol{L}$ = 119 cm, $\boldsymbol{S}$ = 2.31 cm; and for $\boldsymbol{L}$ = 80 cm, $\boldsymbol{S}$ = 3.36 cm. Indeed, as $\boldsymbol{L}$ increases, $\boldsymbol{S}$ decreases.

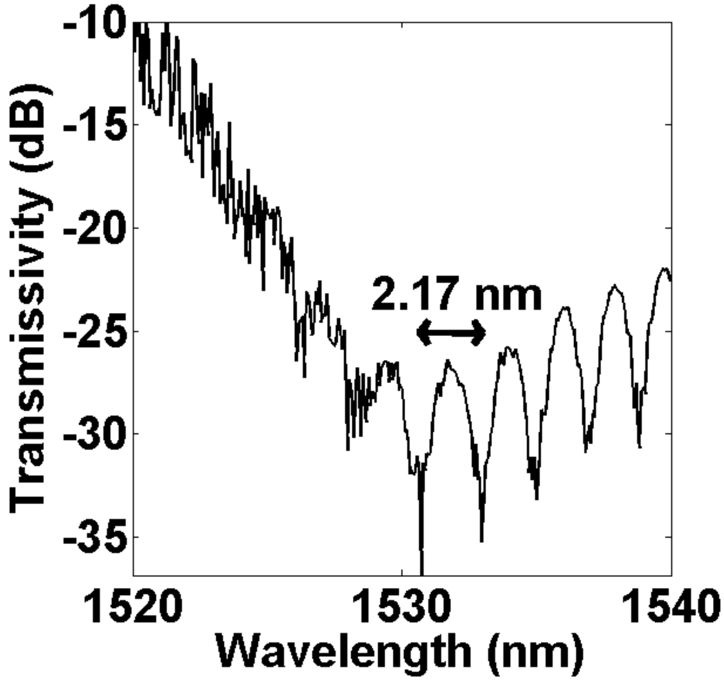
-10
-15
-20
-25
-30
-35
Transmissivity (dB)
2.17 nm
1520
1530
1540
Wavelength (nm)

(a)

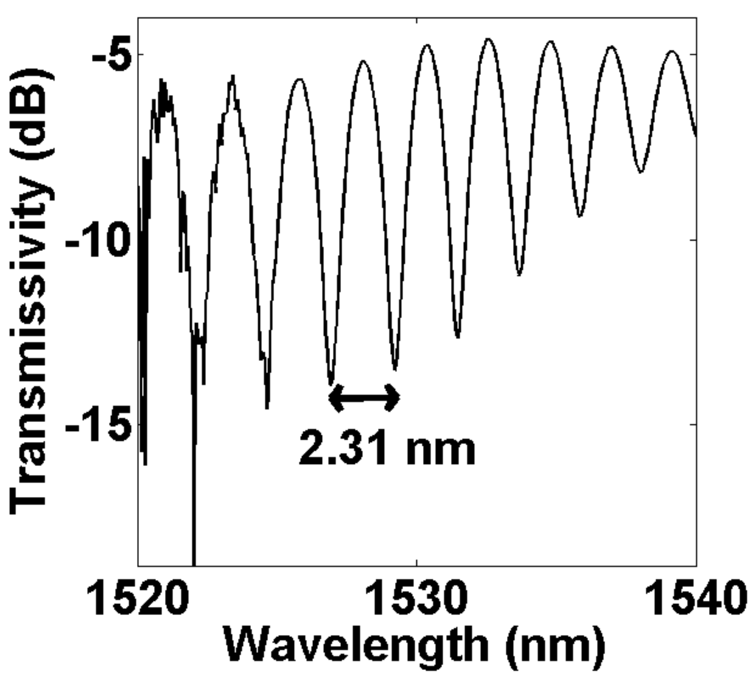
-5
-10
-15
Transmissivity (dB)
2.31 nm
1520
1530
1540
Wavelength (nm)

(b)

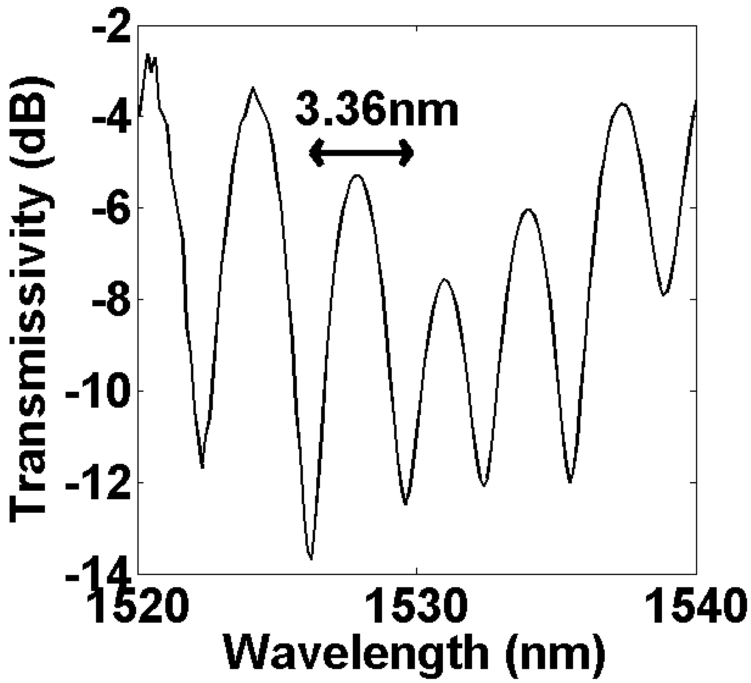

(c)

Figure 5.2 Measured spectral responses of cascaded LPGs with a separation of (a) 133 cm (b) 119 cm (c) 80 cm

Knowing the relationship between $\boldsymbol{S}$ and $\boldsymbol{L}$ from Eq. 5.1, the MZI response can be verified by comparing calculated and measured values. First, for each measurement of $\boldsymbol{S}$ and $\boldsymbol{L}$, $\boldsymbol{\Delta m}$ is calculated. Next, by using one of the values of $\boldsymbol{\Delta m}$, (1) $\boldsymbol{L}$ is determined from the measured $\boldsymbol{S}$ and (2) $\boldsymbol{S}$ is determined from the measured $\boldsymbol{L}$. The comparisons between the calculations and the measurements are summarized in the following tables. In Table 5.1, three values of $\boldsymbol{\Delta m}$ are obtained from each measurement. In Table 5.2-5-4, (1) $\boldsymbol{L}$ and (2) $\boldsymbol{S}$ are then obtained for each value of $\boldsymbol{\Delta m}$. The smallest and the largest differences between the calculations and the measurements are 1.81% and 7.37%, respectively. All these results indicate that $\boldsymbol{S}$ is inversely proportional to $\boldsymbol{L}$ and satisfy Eq. 5.1.

λ	S	L	Δf	$\triangle$m
1.55E-06	2.17E-09	1.33E+00	2.70968E+11	8.32E-04
1.55E-06	2.31E-09	1.19E+00	2.8845E+11	8.74E-04
1.55E-06	3.36E-09	8.00E-01	4.19563E+11	8.94E-04

Table 5.1: Δm calculations based on measured S and L

Measured L (m)	Calculated L (m)	Difference (%)
1.33E+00	1.33E+00	1.67E-14
1.19E+00	1.25E+00	4.99E-00
8.00E-01	8.59E-01	7.37E-00
Measured S (m)	Calculated S (m)	
2.17E-09	2.17E-09	0.00E+00
2.31E-09	2.43E-09	4.99E+00
3.36E-09	3.61E-09	7.37E+00

Table 5.2: L & S comparisons based on calculated $\Delta m = 8.32e - 4$

Measured L (m)	Calculated L (m)	Difference (%)
1.33E+00	1.27E+00	-6.32E+00
1.19E+00	1.19E+00	0.00E+00
8.00E-01	8.18E-01	1.81E+00
Measured S (m)	Calculated S (m)	
2.17E-09	2.07E-09	-4.75E+00
2.31E-09	2.31E-09	0.00E+00
3.36E-09	3.44E-09	2.27E+00

Table 5.3: L & S comparisons based on calculated $\Delta m = 8.74e - 4$

Measured L (m)	Calculated L (m)	Difference (%)
1.33E+00	1.24E+00	-6.86E+00
1.19E+00	1.16E+00	-2.22E+00
8.00E-01	8.00E-01	1.39E-14
Measured S	Calculated S	
2.17E-09	2.02E-09	-6.86E+00
2.31E-09	2.26E-09	-2.22E+00
3.36E-09	3.36E-09	1.23E-14

Table 5.4: L & S comparisons based on calculated $\Delta m = 8.94e - 4$

5.1 Summary

In this chapter, the setup of ZBLAN MZI based on cascaded LPGs is explained. The measured interference patterns are compared to the calculated values. They match reasonably well with an error range from 1.81% to 7.37%.

Chapter 6 - Conclusion

In this thesis, the development of ZBLAN fiber-based components is presented. The material that is superior in the mid-IR is first investigated in the near-infrared. Techniques for fusion splicing (by fusion arc splicer) and fabricating LPGs (by mechanically inducing) and MZIs (by cascading the LPGs) are developed.

In introduction, the motivation is discussed by comparing ZBLAN to silica and by an overview of potential applications in the mid-IR. In background and review, the principle and development of the interested components are presented. In the following chapters, the techniques and the components are successfully demonstrated.

6.1 Future Work

In terms of fusion splicing, it is worth repeating the trials using a different type of splicer, namely a filament splicer. The filament splicer has a greater range of splice settings and its heating element appears more stable during the hot push. Other than the splices presented in this thesis, it is also worth trying to fusion splice among different combinations of ZBLAN fibers, silica fibers, and doped ZBLAN fibers. To improve the splicing between two materials with quite different T_g, it seems important to have a heat profile or zone that can heat each one at respective temperature. It might be interesting to develop such a heating element or a program.

In terms of LPGs, different grating parameters should be tested. Within the limits of available screws, different grating lengths and grating periods can be achieved. The clamp might be improved as well if the advantages of clamp 1 and 2 are combined. Also, the way that the fiber is positioned on the plate can be changed to a U-shape, where the two ends of the fiber sit next to each other on one clamp and one screw. One easy way to improve the setup is by using motorized stages. Other methods of fabricating LPGs, for example arc-induced or UV exposure, are interesting to try.

Besides the same proposed improvements from LPGs, the cascaded LPGs can be connected to ZBLAN-fiber-based broad-band source such as a pumped length of doped ZBLAN fiber (Appendix D) to achieve a spectrally sliced source. Reducing the setup losses is also important.

References

[1] L. R. Chen, Class Lecture, Photonic Devices and Systems, Fall 2008.

[2] W. A. Gambling, "The Rise and Rise of Optical Fibers," IEEE J. Sel. Top. Quant., Vol. 6, No. 6, pp. 1084-1093, Nov/Dec 2000.

[3] D. C. Tran *et al.*, "Heavy Metal Fluoride Glasses and Fibers: A Review," J. Lightwave Technol., Vol. 2, No. 5, pp. 566-586, October 1984.

[4] J. A. Harrington, *Infrared Fibers and their Applications*, SPIE, 2004.

[5] M. Poulain *et al.*, "Verres Fluores au Tetrafluorure de Zirconium Proprietes Optiques d'un Verre Dope au Nd^{3+}," Mater. Res. Bull., Vol. 10, No. 4, pp. 243-246, 1975.

[6] S. F. Carter *et al.*, "Prospects for Ultra-Low-Loss Fluoride Fibres at BTRL," J. Non-Cryst. Solids, Vol. 140, pp. 153-158, 1992.

[7] http://www.iguide-irphotonics.com/pdf/UVIR_glass_janv10.pdf. Last accessed June 2011.

[8] http://www.iguide-irphotonics.com/pdf/multimode_infrared_fiber_january11.pdf. Last accessed June 2011.

[9] http://www.iguide-irphotonics.com/pdf/singlemode_infrared_fiber_august10.pdf. Last accessed June 2011.

[10] http://www.iguide-irphotonics.com/pdf/DSS2009final.pdf. Last accessed June 2011.

[11] A. D. Yablon, *Optical Fber Fusion Splicing*, Springer-Verlag Berlin Heidelberg, 2005.

[12] B. B. Harbison *et al.*, "Fusion Splicing of Heavy Metal Fluoride Glass Optical Fibres," Electron. Lett., Vol. 25, No. 18, pp. 1214-1216, 1989.

[13] B. Srinivasan *et al.*, "Reproducible Fusion Splicing of Low Melting Point (Fluoride) Optical Fibers with the Use of a Stable Heat Source," Proceedings of Optical Fiber Communication Conference, pp.1-2, 1997.

[14] L. Pei *et al.*, "Low Loss Splicing Method to Join Silica and Fluoride Fibers," Proc. SPIE 6781, pp. 67814O.1-67814O.6 (2007); doi:10.1117/12.745490.

[15] A. M. Vengsarkar *et al.*, "Long-Period Fiber Gratings as Band-Rejection Filters, "J. Lightwave Technol., Vol. 14, No. 1, pp. 58-65, 1996.

[16] S. Savin *et al.*, "Tunable Mechanically Induced Long-Period Fiber Gratings," Opt. Lett., Vol. 25, No. 10, pp. 710-712, 2000.

[17] D. Pudo *et al.*, "Long-Period Gratings in Chalcogenide Fibers," Optics Express, Vol. 14, No. 9, pp. 3763-3766, 2006.

[18] J. Shamir, *Optical Systems and Processes*, SPIE, 1999.

[19] http://www.rp-photonics.com/interferometers.html. Last accessed June 2011.

[20] X. J. Gu, “Wavelength-Division Multiplexing Isolation Fiber Filter and Light Source Using Cascaded Long-Period Fiber Gratings,” Opt. Lett., Vol. 23, No. 7, pp. 509-510, 1998.

[21] J. H. Lim *et al.*, “Mach–Zehnder Interferometer Formed in a Photonic Crystal Fiber Based on a Pair of Long-Period Fiber Gratings,” Vol. 29, No. 4, pp. 346-348, 2004.

[22] H. Y. Choi *et al.*, “Photonic Crystal Fiber Interferometer Composed of a Long Period Fiber Grating and One Point Collapsing of Air Holes,” Vol. 33, No. 8, pp. 812-814, 2008.

[23] http://www.rp-photonics.com/fiber_lasers.html. Last accessed June 2011.

[24] B. H. Lee *et al.*, “Dependence of Fringe Spacing on the Grating Separation in a Long-Period Fiber Grating Pair,” Appl. Opt., 38, pp. 3450-3459, 1999.

[25] A. Soibel *et al.*, “Midinfrared Interband Cascade Laser for Free Space Optical Communication,” IEEE Photon. Technol. Lett., Vol. 22, No. 2, pp. 121-123, 2010.

[26] R. Martini *et al.*, “Free-Space Optical Transmission of Multimedia Satellite Data Streams Using Mid-Infrared Quantum Cascade Lasers,” Electron. Lett., Vol. 38, No. 4, pp. 181-183, 2002.

[27] H. Manor *et al.*, “Performance of an Optical Wireless Communication System as a Function of Wavelength,” Appl. Opt., Vol. 42, No. 21, pp. 4285-4294, 2003.

[28] E. Ip *et al.*, "QPSK Transmission over Free-Space Link at 3.8 Microns using Coherent Detection with Wavelength Conversion", Proc. of Euro. Conf. on Optical Commun., Brussels, Belgium, September 21-25, 2008.

[29] D. Ouzounov *et al.*, “Mid-Infrared Emission prior to Strong Earthquakes Analyzed by Remote Sensing Data,” Adv. Space Res., 33 (2004) pp. 268–273.

[30] P. Werle *et al.*, “Near- and Mid-Infrared Laser-Optical Sensors for Gas Analysis,” Opt. Laser. Eng., 37 (2002) pp. 101-114.

[31] T. Topfer *et al.*, “Room-Temperature Mid-Infrared Laser Sensor for Trace Gas Detection,” Appl. Opt., Vol. 36, No. 30, pp. 8042-8049, 1997.

[32] Y. A. Bakhirkin *et al.*, “Mid-Infrared Quantum Cascade Laser Based Off-Axis Integrated Cavity Output Spectroscopy for Biogenic Nitric Oxide Detection,” Appl. Opt., Vol. 43, No. 11, pp. 2257-2266, 2004.

[33] N. Gayraud *et al.*, “Mid-Infrared Gas Sensing Using a Photonic Bandgap Fiber,” Appl. Opt., Vol. 47, No. 9, pp. 1269-1277, 2008.

[34] U. Willer *et al.*, “Near- and Mid-Infrared Laser Monitoring of Industrial Processes, Environment and Security Applications,” Opt. Laser. Eng., 44 (2006) pp. 699–710.

[35] L. Kornaszewski *et al.*, “Mid-Infrared Methane Detection in a Photonic Bandgap Fiber Using a Broadband Optical Parametric Oscillator,” Optics Express, Vol. 15, No. 18, pp. 11219-11224, 2007.

[36] M. Saito *et al.*, “Infrared Optical Fiber Sensors,” Opt. Rev., Vol. 4, No. 5 (1997) pp. 527-538.

[37] B. Guo *et al.*, “Laser-Based Mid-Infrared Reflectance Imaging of Biological Tissues,” Optics Express, Vol. 12, No. 1, pp. 208-219, 2004.

[38] C. Roller *et al.*, “Simultaneous NO and CO2 Measurement in Human Breath with a Single IV–VI Mid-Infrared Laser,” Opt. Lett., Vol. 27, No. 2, pp. 107-109, 2002.

[39] R. W. Waynant *et al.*, Mid-Infrared Laser Applications in Medicine and Biology,” Phil. Trans. R. Soc. Lond. A, (2001) 359, pp. 635–644.

[40] K. Chen *et al.*, “Several Mechanically-Induced Long-Period Gratings by a Grooved Plate,” Chinese Optics Letters, Vol. 1, Issue 8, pp. 444-446 (2003).

[41] K. Chen *et al.*, “Band-Rejection and Bandpass Filters based on Mechanically Induced Long-Period Fiber Gratings,” Microw. Opt. Techn. Let., Vol. 42, Issue 1, pp. 15-17 (2004).

[42] H. Ke *et al.*, "Analysis of Phase-Shifted Long-Period Fiber Gratings," IEEE Photon. Technol. Lett., Vol. 10, No. 11, pp. 1596-1598, 1998.

[43] B. Jean *et al.*, “Mid-IR Laser Applications in Medicine,” Solid-State Mid-Infrared Laser Sources, Topics in Applied Physics, 89, pp. 511–546 (2003).

[44] J. S. Nelson *et al.*, “Mid-Infrared Erbium:YAG Laser Ablation of Bone: The Effect of Laser Osteotomy on Bone Healing,” Lasers in Surgery and Medicine, Vol. 9, No. 4, pp. 362-374 (1989).

[45] Q. Ren *et al.*, “Mid-Infrared Laser Ablation of the Cornea: A Comparative Study,” Lasers in Surgery and Medicine, Vol. 12, No. 3, pp. 274-281 (1992).

[46] H. Poignant *et al.*, “Effeciency and Thermal Behavior of Cerium Doped Fluorozirconate Glass Fiber Bragg Gratings,” Electronics Letters, Vol. 30, No. 16, pp. 1339-1341, 1994.

[47] T. Taunay *et al.*, “Ultraviolet-Induced Permanent Bragg Gratings in Cerium-Doped ZBLAN Glasses or Optical Fibers”, Optics Letters, Vol. 19, No. 17, pp. 1269-1271, 1994.

[48] D. Grobnic *et al.*, “Femtosecond IR Laser Inscription of Bragg Gratings in Single- and Multimode Fluoride Fibers,” IEEE Photonics Technology Letters, Vol. 18, No. 24, pp. 2686-2688, 2006

[49] M. Bernier *et al.*, “Bragg Gratings Photoinduced in ZBLAN Fibers by Femtosecond Pulses at 800 nm,” Optics Letters, Vol. 32, No. 5, pp. 454-456, 2007

Appendix A – Fusion Splicing Settings

Figure A.1: Fusion splicing settings 1

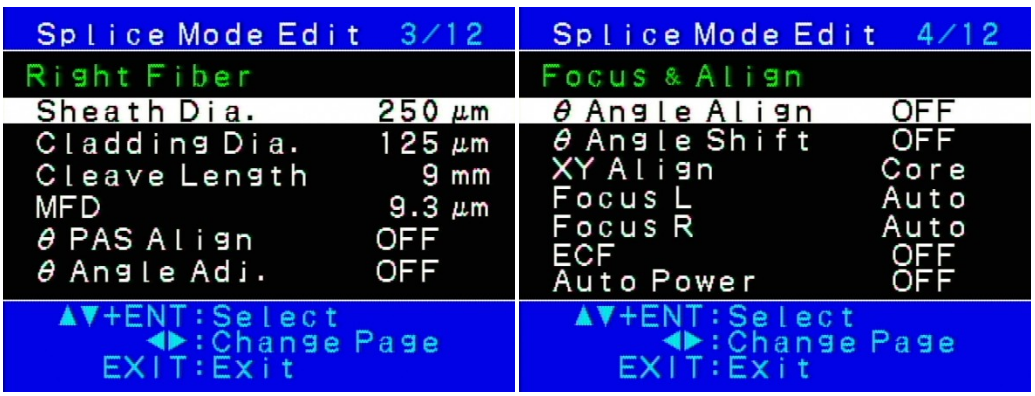

Figure A.2: Fusion splicing settings 2

Figure A.3: Fusion splicing settings 3

Figure A.4: Fusion splicing settings 4

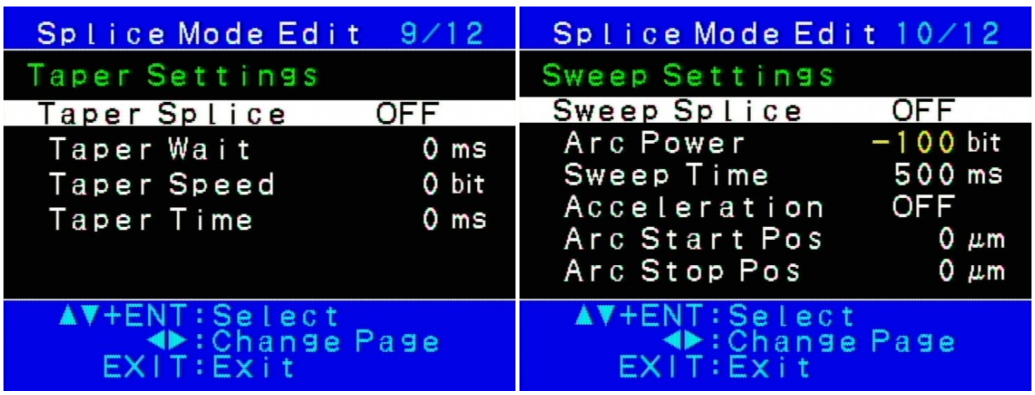

Figure A.5: Fusion splicing settings 5

Figure A.6: Fusion splicing settings 6

Appendix B – LPG Simulation

B.1 MATLAB Code for LPG 2 Simulation

```
% Modeling of Long-Period Grating by Hsin-yu Lu from McGill University
% Photonics System Group in 2011 for Master of Engineering

% Version 1
% LPG at 1550 nm

% References
% H. Ke et al., "Analysis of Phase-Shifted Long-Period
% Fiber Gratings," IEEE PHOTONICS TECHNOLOGY LETTERS, VOL. 10, NO. 11,
% NOVEMBER 1998.

% Parameters
L = 25.4e-3; % grating length = 25.4 mm
period = 0.639e-3; % grating period = 0.71 mm, 10% difference
peak = 1550e-9; % peak wavelength
delta_neff = peak/period; % effective index difference for a selected
peak
n_core = 1.491;
n_clad = 1.476;
n_avg = (n_core+n_clad)/2;
overlap = 0.62; % assumed
n_pert = 1.5848e-4; % amplitude of perturbation

% F-Matrix Method [1]
for x = 1:301
    wavelength2(x) = 1520e-9 + 60e-9*(x-1)/300;
    delta(x) = (1/2)*(2*pi/wavelength2(x))*(delta_neff) - (pi/period);
% phase mismatch
    kappa(x) = (2*pi/wavelength2(x))/(4*n_avg)*(overlap)*(n_pert); %
coupling coefficient
    gamma(x) = sqrt(delta(x)^2+kappa(x)^2);
    T3(x) = (cos(gamma(x)*L))^2 + (delta(x)/gamma(x))^2 *
(sin(gamma(x)*L))^2;
end
% Plot
figure(1)
plot(wavelength2*1e9,T3,'r');
title('Simulated ZBLAN LPG Response in C-band')
xlabel('Wavelength (nm)');
ylabel('Normalized Transmissivity');
axis tight;
```

Appendix C – LPG in MM Regime

The V-number of the SM ZBLAN fiber at 1550 nm is 3.101. Fig. C.1 shows that two modes propagate in the core of this weakly guiding fiber: LP_{01} and LP_{11}. It is important to verify whether the LPG couples the light from the core to the cladding instead of between these two modes.

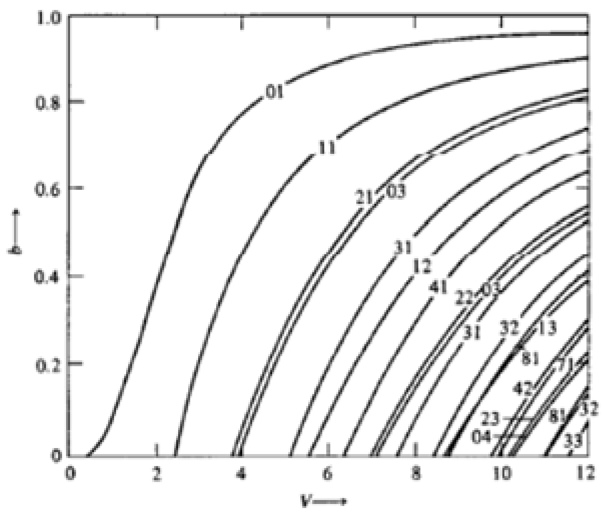

Figure C.1: b-V curve for weakly guiding fiber [C1]

From the estimations of the normalized propagation constants in Fig. C.1, the grating period required to couple between the LP_{01} and the LP_{11} modes is approximately 359 μm, which is 49.4% away from the grating period of LPG_2 and even farer from that of LPG_1. As a result, it is safe to assume that the coupling between the core modes does not occur.

[C1] L. R. Chen, Class Lecture, Optical Waveguides, Fall 2009.

Appendix D - Doped ZBLAN Fiber

The objective of this experiment is to measure the amplified spontaneous emission (ASE) from a Tm-ZBLAN fiber in the S-band. The ASE can then be used for making light sources. Fig. D.1 illustrates the experimental setup. A pump laser at 1064 nm is used to trigger the emission around 1480 nm. The doped ZBLAN fiber ends are connected to silica fiber ends via a glue splicing technique. The fiber is co-doped with 36700 ppm of cerium (Ce) and 2600 ppm of thulium (Tm). It has a core diameter of 10 μm, a cladding diameter of 125 μm, and NA of 0.2. An OSA is connected at the end to measure the ASE spectrum.

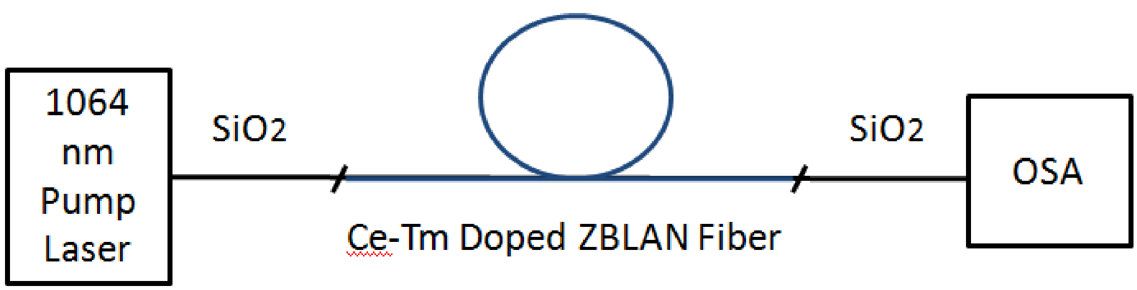

Figure D.1: Experimental setup of ASE measurement

Fig. D.2 shows the ASE spectrum for a launch pump power of 330 mW observed from the OSA. The ASE peak is located at -62.36 dBm near 1472.4 nm. The fiber length is estimated to be 5 m. To improve the pump efficiency, a few things are looked at. As described by Komukai *et al.*, smaller core diameter leads to higher pump efficiencies [D1]. However, a smaller core also causes lower transparency powers. Therefore, combining with the variable fiber length, there should be an optimized length and core diameter to get the most of ASE possible.

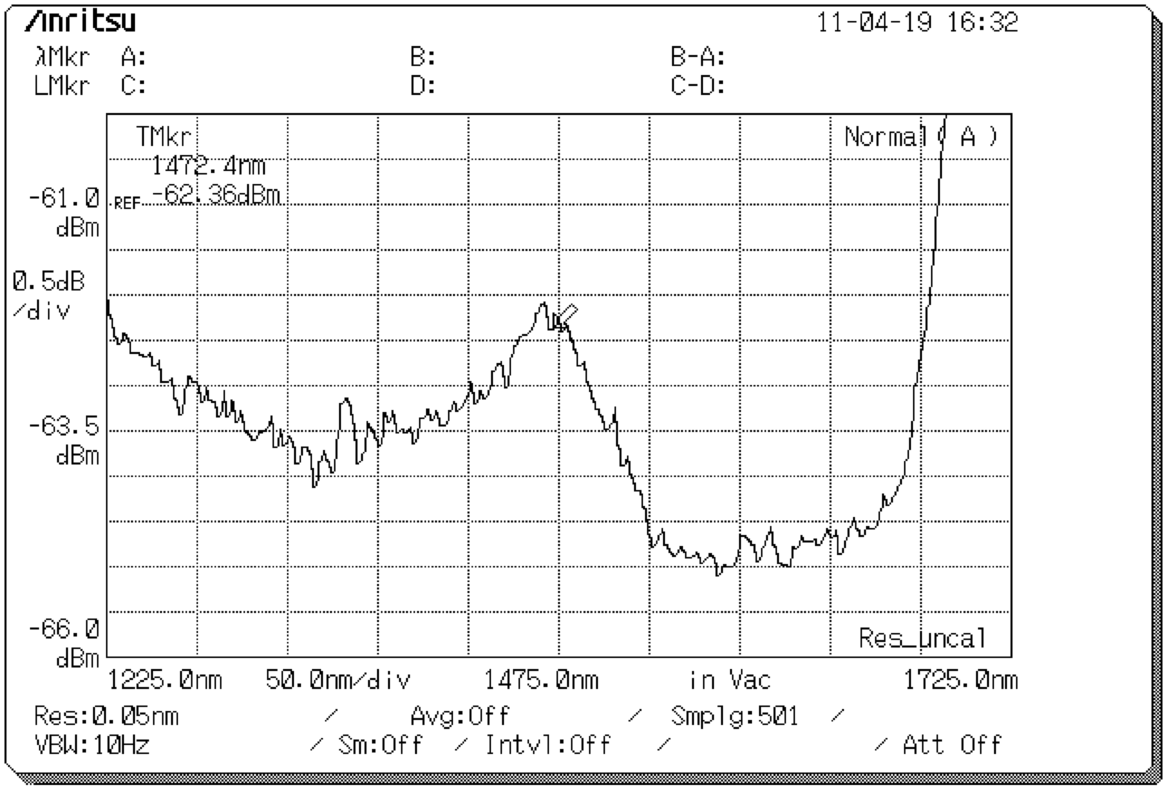

Figure D.2: Measured ASE from the Ce-Tm doped ZBLAN fiber

Another ASE experiment has been performed on a different doped fiber. The fiber in use has a 6.05 m length, 6 μm core diameter, 125 μm cladding diameter, 0.2 NA, and 4000 ppm Tm concentration (without Ce this time). Fig. D.3 shows the measured ASE. At a launch power of 3033 mW, the ASE peak is -40.54 dBm around 1465 nm.

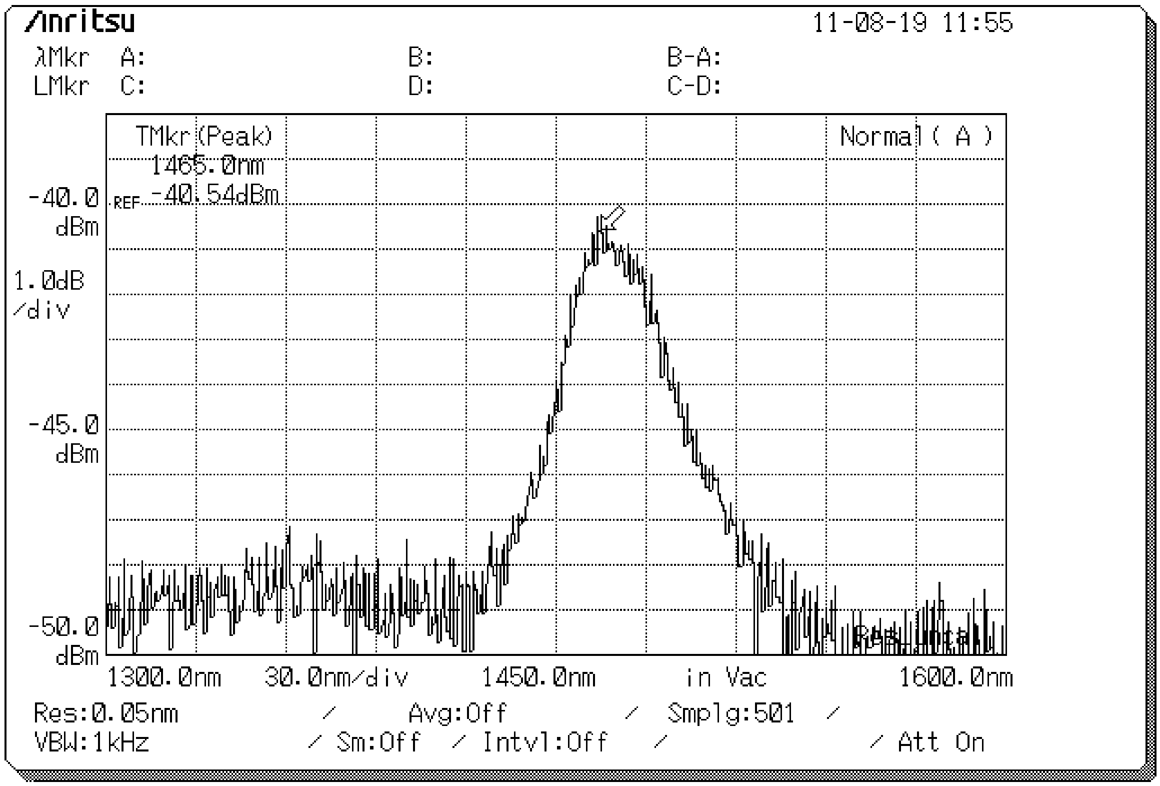

Figure D.3: ASE spectrum from 1064-nm-pumped Tm-doped ZBLAN fiber

[D1] T. Komukai *et al.*, "Upconversion Pumped Thulium-Doped Fluoride Fiber Amplifier and Laser Operating at 1.47 μm," IEEE J. Quantum Electron., Vol. 31, No. 11, pp. 1880-1889, 1995.